

Institutionen för systemteknik

Department of Electrical Engineering

Examensarbete

Fault Diagnosis of a Fixed Wing UAV Using Hardware and Analytical Redundancy

Examensarbete utfört i Fordonssystem
vid Tekniska högskolan vid Linköpings universitet
av

Michael Andersson

LiTH-ISY-EX--13/4661--SE

Linköping 2013



Linköpings universitet
TEKNISKA HÖGSKOLAN

Fault Diagnosis of a Fixed Wing UAV Using Hardware and Analytical Redundancy

Examensarbete utfört i Fordonssystem
vid Tekniska högskolan vid Linköpings universitet
av

Michael Andersson

LiTH-ISY-EX--13/4661--SE

Handledare: **Emil Larsson**
ISY, Linköpings universitet
Thom Magnusson
Instrument Control Sweden

Examinator: **Mattias Krylander**
ISY, Linköpings universitet

Linköping, 17 maj 2013

	Avdelning, Institution Division, Department Institution for Vehicular Systems Department of Electrical Engineering SE-581 83 Linköping	Datum Date 2013-05-17
	Språk Language <input type="checkbox"/> Svenska/Swedish <input checked="" type="checkbox"/> Engelska/English <input type="checkbox"/> _____	Rapporttyp Report category <input type="checkbox"/> Licentiatavhandling <input checked="" type="checkbox"/> Examensarbete <input type="checkbox"/> C-uppsats <input type="checkbox"/> D-uppsats <input type="checkbox"/> Övrig rapport <input type="checkbox"/> _____
URL för elektronisk version http://urn.kb.se/resolve?urn=urn:nbn:se:liu:diva-XXXXX		
Titel Title	Feldiagnos av obemannat flygplan genom hårdvaru- och analytisk redundans Fault Diagnosis of a Fixed Wing UAV Using Hardware and Analytical Redundancy	
Författare Author	Michael Andersson	
Sammanfattning Abstract	<p>In unmanned aerial systems an autopilot controls the vehicle without human interference. Modern autopilots use an inertial navigation system, GPS, magnetometers and barometers to estimate the orientation, position, and velocity of the aircraft. In order to make correct decisions the autopilot must rely on correct information from the sensors.</p> <p>Fault diagnosis can be used to detect possible faults in the technical system when they occur. One way to perform fault diagnosis is model based diagnosis, where observations of the system are compared with a mathematical model of the system. Model based diagnosis is a common technique in many technical applications since it does not require any additional hardware. Another way to perform fault diagnosis is hardware diagnosis, which can be performed if there exists hardware redundancy, i.e. a set of identical sensors measuring the same quantity in the system.</p> <p>The main contribution of this master thesis is a model based diagnosis system for a fixed wing UAV autopilot. The diagnosis system can detect faults in all sensors on the autopilot and isolate faults in vital sensors as the GPS, magnetometer, and barometers. This thesis also provides a hardware diagnosis system based on the redundancy obtained with three autopilots on a single airframe. The use of several autopilots introduces hardware redundancy in the system, since every autopilot has its own set of sensors. The hardware diagnosis system handles faults in the sensors and actuators on the autopilots with full isolability, but demands additional hardware in the UAV.</p>	
Nyckelord Keywords	Fault Diagnosis, Model based diagnosis, Redundancy, Autopilot, UAV, fixed-wing	

Sammanfattning

I obemannade flygsystem styr en autopilot farkosten helt autonomt. Moderna autopiloter använder tröghetnavigering, GPS, magnetometrar och barometrar för att skatta farkostens orientering, position och hastighet. För att autopiloten ska kunna fatta korrekta beslut måste informationen från dessa sensorer vara tillförlitlig. I det här examensarbetet utvecklas ett modellbaserat diagnosystem för att detektera fel i autopilotens sensorer.

Ett diagnosystem kan användas för att detektera eventuella fel som kan uppstå i tekniska system. Ett sätt att designa ett diagnosystem är genom modellbaserad diagnos där observationer i systemet jämförs med en matematisk modell. En fördel med modellbaserad diagnos är att det inte krävs någon extern hårdvara, utan endast en matematisk modell av systemet. Ett annat sätt att designa ett diagnosystem är genom hårdvarudiagnos, där en uppsättning av identiska sensorer används för att mäta samma storheter.

Huvudbidraget i detta examensarbete är ett modellbaserat diagnosystem för autopiloter till förarlösa flygplan. Diagnosystemet kan detektera fel i alla autopilotens sensorer och isolera fel i viktiga sensorer som GPS, magnetometer och barometer. I arbetet utvecklas också ett hårdvarudiagnosystem bestående av tre autopiloter, utrustade med en identisk uppsättning av sensorer. Genom att använda tre autopiloter på samma farkost introducerar man hårdvaruredundans i systemet. Hårdvarudiagnosystemet kan hantera enkelfel i alla sensorer och aktuatorer på samtliga autopiloter med full isolerbarhet, men ställer samtidigt krav på extern hårdvara.

Abstract

In unmanned aerial systems an autopilot controls the vehicle without human interference. Modern autopilots use an inertial navigation system, GPS, magnetometers and barometers to estimate the orientation, position, and velocity of the aircraft. In order to make correct decisions the autopilot must rely on correct information from the sensors.

Fault diagnosis can be used to detect possible faults in the technical system when they occur. One way to perform fault diagnosis is model based diagnosis, where observations of the system are compared with a mathematical model of the system. Model based diagnosis is a common technique in many technical applications since it does not require any additional hardware. Another way to perform fault diagnosis is hardware diagnosis, which can be performed if there exists hardware redundancy, i.e. a set of identical sensors measuring the same quantity in the system.

The main contribution of this master thesis is a model based diagnosis system for a fixed wing UAV autopilot. The diagnosis system can detect faults in all sensors on the autopilot and isolate faults in vital sensors as the GPS, magnetometer, and barometers. This thesis also provides a hardware diagnosis system based on the redundancy obtained with three autopilots on a single airframe. The use of several autopilots introduces hardware redundancy in the system, since every autopilot has its own set of sensors. The hardware diagnosis system handles faults in the sensors and actuators on the autopilots with full isolability, but demands additional hardware in the UAV.

Acknowledgments

I would like to thank ICS for providing the opportunity to work with this master thesis and the staff at ICS for all help and support. A special thanks to my supervisor Thom Magnusson for all the technical support and useful ideas. Special thanks also to my supervisor Emil Larsson and examiner Mattias Krysander at ISY for all the fruitful discussions and the valuable feedback on this report. I would also like to thank my opponent and friend Per Boström for feedback and discussions during the work.

*Michael Andersson
Linköping, May 2013*

Contents

Notation	xiii
----------	------

I Introduction

1 Introduction	3
1.1 Background	3
1.1.1 Instrument Control Sweden	3
1.1.2 Commercial Unmanned Aerial Vehicles	5
1.2 Related Research	6
1.2.1 Modeling	6
1.2.2 Attitude Estimation	6
1.2.3 Control System	6
1.2.4 Navigation	7
1.2.5 Diagnosis System	7
1.3 Aims and Problem Formulation	7
1.4 Outline	8

II Theory

2 Fault Diagnosis	13
2.1 Redundancy	13
2.2 Residuals	14
2.3 Fault Modes	15
2.4 Diagnosis Tests	17
2.4.1 Structural Analysis	18
2.5 Fault Detection	19
2.5.1 Thresholding	19
2.5.2 Filtering	19
2.5.3 Change Detection	20
2.6 Decision Logic	21

3	Coordinate Systems	23
3.1	Earth-centered and Earth-fixed	23
3.2	Local Geodetic Frame	24
3.3	Body Frame	25
3.4	Rotation Between Frames	25
3.4.1	Quaternions	26
4	Sensors	31
4.1	Gyroscopes	31
4.1.1	Performance	31
4.1.2	Statistical Analysis	32
4.1.3	Calibration	32
4.2	Accelerometers	33
4.2.1	Performance	33
4.2.2	Statistical Analysis	33
4.2.3	Calibration	33
4.3	Magnetometer	34
4.3.1	Performance	34
4.3.2	Calibration	35
4.4	Pressure Sensors	37
4.4.1	Performance	38
4.4.2	Calibration	38
4.5	Global Navigation Satellite System	38
4.5.1	Position Estimation	38
4.5.2	Speed and Direction Estimation	39
5	Modeling	41
5.1	Attitude Estimation Model	42
5.1.1	Accelerometers	42
5.1.2	Magnetometers	43
5.1.3	Gyroscopes	44
5.1.4	GPS	44
5.2	Height Estimation Model	45
5.2.1	GPS	45
5.2.2	Static Pressure Sensor	45
5.3	Velocity Estimation Model	45
5.3.1	Ground Speed	46
5.3.2	Air Speed	46
5.4	Position Estimation Models	46
5.4.1	GPS	47
5.5	Summarized Model	47
5.5.1	Measurements Equations with Faults	47
5.5.2	System Equations	48

III Results

6	Model Based Diagnosis System	51
6.1	System Structure	51
6.2	Workflow	51
6.3	Results	52
6.3.1	MTES Test Candidates	53
6.3.2	TES Test Candidates	54
6.3.3	Final Set of Tests	54
6.3.4	Residual generation	55
7	Triple Redundant Autopilot	67
7.1	Components	67
7.1.1	Autopilot	67
7.1.2	Supervisor Unit	68
7.1.3	Modem	68
7.1.4	Servo	68
7.2	Communication	68
7.2.1	Sensor Data and Estimated States	68
7.2.2	Control Signals and Servo	68
7.2.3	Diagnosis Data	69
7.2.4	Modem Communication	69
7.2.5	Synchronization	70
7.2.6	Controller Area Network	70
7.3	Hardware Diagnosis	71
7.3.1	Fault Modes	71
7.3.2	Diagnosis Tests	72
7.3.3	Voting	74
7.3.4	Detectability and Isolability	74
8	Conclusions and Future Work	77
8.1	Conclusions	77
8.1.1	Model Based Diagnosis System	77
8.1.2	Triple Redundant Autopilot	78
8.2	Future Work	79
8.2.1	Improved Isolability	79
8.2.2	Other Fault Sources	79
8.2.3	Multiple Faults	79
8.2.4	Backup Filter	79
8.2.5	Simulator and Simulink Model	79
A	Appendix	81
A.1	Vincenty's Formula	81
A.2	Plots	81
	Bibliography	89

Notation

ACRONYMS

Acronym	Meaning
AHRS	Attitude heading reference system
CAN	Controller area network
CUSUM	Cumulative Sum
ECEF	Earth-centered, earth-fixed
EKF	Extended Kalman filter
FIR	Finite impulse response
GCS	Ground control system
GNSS	Global navigation satellite system
GPS	Global positioning system
ICS	Instrument control Sweden
LGF	Local geodetic frame
MBDS	Model based diagnosis system
MEMS	Micro-electro-mechanical system
MISO	Minimal structurally overdetermined
MTES	Minimal test equation support
NED	North east down
PSO	Proper structurally overdetermined
RLS	Recursive least square
SU	Sensor unit
TDOA	Time difference of arrival
TES	Test equation support
TOA	Time of arrival
TS	Test support
TRA	Triple redundant autopilot
UAV	Unmanned aerial vehicle
WGS	World geodetic system

Part I

Introduction

1

Introduction

For expensive airframes a diagnosis system that can handle faults in the autopilot is desirable. Without a diagnosis system a vital fault in the autopilot will most likely imply a crash landing of the UAV. One possible way to increase the reliability of the UAV is to use several autopilots on a single airframe. The use of several autopilots introduces hardware redundancy in the system, since every autopilot has its own set of sensors. The idea of this thesis is to investigate how a diagnosis system for fixed wing UAVs can be designed using both hardware and analytical redundancy.

This report presents the work in the master thesis *Fault diagnosis of a fixed wing UAV using analytical and hardware redundancy*. The thesis has been performed at Instrument Control Sweden AB and the division of Vehicular Systems, the department of Electrical Engineering at Linköping University. The purpose of this report is to present the work and the result of the master thesis. This section describes the background and the problem formulation of the work.

1.1 Background

This section describes the background of Instrument Control Sweden and the use of unmanned aerial vehicles (UAVs).

1.1.1 Instrument Control Sweden

Instrument Control Sweden (ICS) is a company located in Linköping, started in 2002. ICS operates in two different areas, consultancy work for the US Air Force, and developing and sell complete solutions for UAV operation with ground control stations, autopilot and high end software. ICS have developed several prod-

ucts in their SkyView series. All of these are adapted to the NATO STANAG 4586 standard for UAV communication.

- **SkyView GCS** Is an unmanned aircraft system, which allows the user to control and monitor several UAV's. In SkyView the user decides what the UAV should do. The user can choose to control the UAV in mission or stabilized mode. In mission mode a flight path consisting of waypoints is uploaded to the autopilot. In stabilized mode the user direct control the UAV through the ground station. A screen shot from SkyView GCS is shown in Figure 1.1
- **SkyView GCS portable computer** Is a portable ruggedized computer solution which allow a single operator to handle all tasks related to flying an unmanned aircraft. The computer contains a data modem and foldable antenna for simple UAV communication. Standard operating capability is seven hours. Figure 1.2 shows the portable computer.
- **SkyView EasyPilot 3.0** Is an easy to use miniature autopilot for UAVs. All necessary sensors including 3-axis gyros and accelerometers, low-latency GPS, barometers are integrated on the circuit board. The EasyPilot supports multiple flight modes including missions, loitering and several semi-manual modes. SkyView EasyPilot is shown in Figure 1.3



Figure 1.1: SkyView GCS



Figure 1.2: The SkyView GCS portable computer



Figure 1.3: The SkyView EasyPilot 3.0

1.1.2 Commercial Unmanned Aerial Vehicles

Traditionally UAVs have been limited mainly to military use as they are in general very expensive and there is a great concern for the safety of flying UAVs in civilian skies. The first UAV was developed during the first world war. These UAVs were controlled remotely from the ground and were used as target drones to train anti air crews. Due to concerns about losing pilots during high-risk missions the

United States air force started the development of the first conventional UAV in 1959. At this time the sensors and computers that are needed to build a UAV, was very expensive and came with very poor performance compare to today. The UAV had to rely only on an internal navigation system, using accelerometers and rate gyros to determine attitude, position and velocity.

The modern UAV was born along with the technical improvements of the last decades, in particular the GPS but also high precision gyroscopes and accelerometers. When the high precision components dropped in price, the civilian market for UAVs started to grow. Today, UAVs are used in many civilian applications such as large land area monitoring, oil- and mineral exploration, and transport.

1.2 Related Research

The autopilot is a system to guide the UAV in flight with no assistance from human operators. A lot of work have been done in the field of autopilots for fixed wing UAVs. The fundamentals of UAV dynamics and flight control are discussed in Chao et al. [2007]. The design of the autopilot can be divided into different subareas:

1.2.1 Modeling

The mathematical model defines the relation between in and outputs to the UAV system. The main approach is to use the laws of motion under assumption that the airframe is a rigid body to obtain dynamic equations of the aircraft. Modeling of an UAVs is done in Tadeo Espinoza and Llama [2013]. An alternative approach is to use system identification to estimate parameters in the different model structures using collected flight data, which is discussed in Gururajan et al. [2012].

1.2.2 Attitude Estimation

The Attitude Heading Reference System (AHRS) uses data from the Sensor Unit (SU) to estimate the attitude of the aircraft. Since the SU have intrinsic error sources it is important to take these errors into account. Several Algorithms based on the Extended Kalman Filters (EKF) have been evaluated in Lima and Tôrres [2012]. Algorithms based on the EKF is evaluated in Magnusson [2013]. Other filters, as for example a explicit complementary filter, are evaluated in Veiback [2010].

1.2.3 Control System

The control system is a very central part of the autopilot. The control system should provide the control signals to the servos and the actuator in the aircraft. Due to high nonlinearities in the aircraft dynamics, the task is not trivial. A lot of intelligent control techniques as PID control, fuzzy logic, Model Predictive Control (MPC), and optimal control have been used in Tadeo Espinoza and Llama [2013] and Kang and Hedrick [2009].

1.2.4 Navigation

The navigation unit estimates the position and velocity on the UAV in a global reference frame. Usually, a GPS is used to estimate the global position and ground speed. In the field of sensor fusion, see Gustafsson [2010], there have been a lot of research to refine the GPS estimate by fusing it with data from other sensors as gyroscopes, accelerometers, and barometers. This is discussed in Sasiadek and Hartana [2004].

1.2.5 Diagnosis System

The diagnosis system is used to detect and isolate possible fault on the autopilot and hence increase the reliability on the autopilot. The fault detection and diagnosis logic is based primarily on the use of redundancy. Analytical redundancy involves the use of a mathematical model of the system and the relationship between the sensor outputs, see Blanke [2003]. Hardware redundancy is based on a comparison between the measurements from identical sensors, measuring the same quantity. The design of diagnosis systems for UAVs based on both hardware and analytical redundancy is discussed in Magrabi and Gibbens [2000]. For a similar system, an autonomous helicopter, a model based diagnosis system with observer-based residual generation is evaluated in Heredia et al. [2005]. The reliability analysis for unmanned autonomous systems is discussed in terms of fault trees and statistics in Remenyte-Prescott et al. [2010].

1.3 Aims and Problem Formulation

Estimates of the heading, position, and velocity are required to control the UAV. If the estimates are poor the system performance will be poor as well, no matter how good the control algorithms are. On the EasyPilot the estimates are delivered by the sensor unit. To improve the estimates from the sensor unit, filtering algorithms such as the EKF could be applied. However, the EKF can't detect a possible error in a specific sensor. If a sensor stops working during a flight, the estimates will be poor.

The main goal of the thesis is to design a model based diagnosis systems for fixed wing UAVs. The diagnosis system should be able to detect faults in sensors on the autopilot and it is desirable that the faults are isolable. The main challenges of this work are:

- **Modeling:** To be able to perform model based diagnosis a mathematical model of the system is needed. The model should consist of dynamic equations describing the motion of the aircraft, measurement equations where faults are introduced, and algebraic equations to describe the relationship between states. The more information about the system that is included in the model, the more redundancy can be used to perform diagnosis.
- **Residual generation:** Residual generation are the task of combining equations in the model to form a residual which is sensitive to a certain set of

faults. The task of decoupling faults in the sensors used to estimate the three dimensional orientation of the aircraft, i.e. the accelerometer, magnetometer, and gyroscopes, will be challenging since all of these sensors are used in the attitude estimation filter on the autopilot.

- **Test evaluation:** Since there are no simulator available in this project, the test can only be evaluated using logged data from real flights. Hence it might become challenging to validate all tests properly.

The secondary goal of this thesis is to design a diagnosis system based on hardware redundancy. The hardware redundancy is introduced by the use of three autopilots on a single airframe. The diagnosis system shall be able to detect a possible single fault in one of the autopilots. If the diagnosis system detects that an autopilot is not working properly, the system should neglect the control signal from this particular autopilot. The diagnosis system should be able to detect and be fault tolerant to some of these faults:

- **Sensor faults:** Faults as bias faults, gain faults, noisy sensors, or dead sensors.
- **Hardware faults:** Faults that could make the autopilot freeze, switch off, or reboot. The battery voltage is critical to monitor, particular in cold climates when the battery is discharged faster than usual.
- **Actuator faults:** Faults in the control signals to the servos.

The system should be designed and tested in MATLAB and partly implemented on a real autopilot. Consequently the main focus of this thesis will be on diagnosis, signal processing and system engineering. The autopilot used in this thesis is the SkyView EasyPilot 3.0, developed by ICS. ICS provides three EasyPilots and logged sensor data as a development tool. The EasyPilot has been developed with the intention of being easily adaptable to different types of fixed wing UAVs with as little calibration and tuning as possible. It is therefore desirable to minimize any added effort of tuning the diagnosis system on the EasyPilot.

1.4 Outline

The thesis includes the following chapters:

Chapter 1, Introduction: An introduction to the work and the background of the project.

Chapter 2, Fault Diagnosis: Describes the concepts of fault diagnosis which is needed to understand the issues in the thesis.

Chapter 3, Coordinate Systems: Describes the coordinate systems that are common in avionics.

Chapter 4, Sensors: Describes the sensors on the EasyPilot.

Chapter 5, Modeling: Presents the model of the UAV system.

Chapter 6, Model Based Diagnosis System: Presents the developed model based diagnosis system.

Chapter 7, Triple Redundant Autopilot: Presents the designed hardware diagnosis system.

Chapter 8, Conclusions and Future Work: Present the conclusions of this works and suggestions for further development.

Part II

Theory

2

Fault Diagnosis

This chapter describes the theory of fault diagnosis which is necessary for understanding the issues in the thesis. Diagnosis of technical system is in general about detecting and isolate possible faults in the system. A fault is defined as an unexpected change that leads to undesirable behavior of the overall performance of the system (Magrabi and Gibbens [2000]). Diagnosis techniques are used in a wide spectrum of applications, in particular automotive systems, Nyberg [1999], and the process industry, Venkatasubramanian et al. [2003]. The task of handling faults detected by the diagnosis system is referred to as fault handling. Depending on the application it might be desirable to warn the operator that a fault is detected, to force the system to enter a backup mode, or force a total stop in the system.

2.1 Redundancy

To be able to perform diagnosis, some kind of extra knowledge about the system is needed. This extra knowledge is called redundancy. Redundancy can be obtained in different ways:

- Extra hardware, for example several sensors measuring the same quantity.
- Sensors in combination with a mathematical model of the system.
- Expertise and experience of the system.

Depending on the characteristics of the system different forms of redundancy may be obtained.

2.2 Residuals

Residuals are generated by a function $f(u, y)$ called a residual generator, where u and y are known signals. The residual generators are made from a mathematical model of the system. Residuals under normal conditions are small and zero mean. The occurrence of a fault causes the residuals to go to a non-zero value.

In real applications the model of the system contains model uncertainty and measurements noise. This means that the residuals in most cases slightly deviate from zero even when the real system has no faults, which may lead to an alarm, i.e. a false alarm. To avoid false alarms the residuals are often filtered and thresholded. When using a high threshold faults may be undetected, but a low threshold may cause false alarms. The principle of residual generation in hardware diagnosis and model based diagnosis is illustrated in Figure 2.1 and Figure 2.2 respectively.

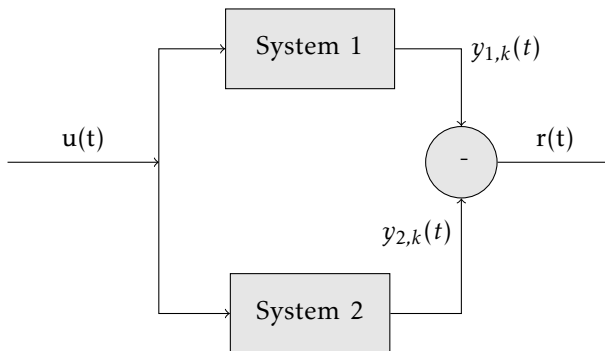


Figure 2.1: The principle of residual generation using hardware diagnosis with identical systems. Several identical sensors in the systems are measuring the same quantity. Pairwise differences from the measurements are created. In this figure, the number of sensors measuring the same quantity $N = 2$.

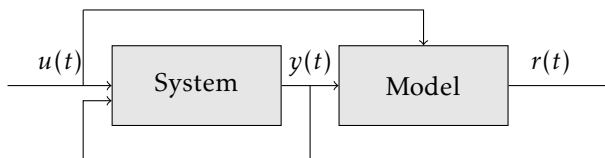


Figure 2.2: The idea of model based residual generation. $r(t)$ is the residual, $y(t)$ are measurements, and $u(t)$ are control signals.

2.3 Fault Modes

Different faults in the system can be classified into different fault modes. The fault-state space Θ is the set of all possible fault modes. Each fault can be classified into a fault mode γ which is associated with a subset Θ_γ of Θ . The fault-free case corresponds to the fault mode "no fault" or **NF**. All subsets Θ_γ are pairwise disjoint, i.e. only one fault mode can be present at the same time. Formal definitions of fault detection and fault isolation can be defined in the terms of fault modes, according to Nyberg [1999].

2.1 Definition. Fault Detection is the task to determine if the system fault-mode **NF** can explain the behavior of the system or not. _____

2.2 Definition. Fault Isolation is the task to determine which system fault-mode that can best explain the behavior of the system. _____

In the MBDS only sensor faults in the autopilot will be considered. A sensor fault is present when the quantity measured by the sensor differs from the true value of the quantity. There are several kind of sensor faults that may affect the autopilot:

Bias fault - When a bias fault is present the signal measured by the sensor is the true signal disturbed by an offset, called a bias. A bias fault can be modeled as

$$y_{meas} = y + b \quad (2.1)$$

where b represents a constant bias in the sensor.

Gain fault - When a gain fault is present the signal measured by the sensor is disturbed by a constant gain. A gain fault can be modeled as

$$y_{meas} = k_{gain} \cdot y \quad (2.2)$$

where k_{gain} represent the gain factor.

Variance fault - When a variance fault is present the signal measured by the sensor measures the true signal disturbed by some noise. A variance fault can be modeled as

$$y_{meas} = y + e \quad (2.3)$$

where the measurement noise e often is modeled as white noise. Measurement noise will always be present in this type of applications. If the amount of measurement noise is low, the true signal and the measurement noise can be distinguished by filtering algorithms on the autopilot. If the amount of

measurement noise is too high the filtering algorithm will not manage to separate the true signal and the measurement noise.

Frozen sensor fault - When a frozen sensor fault is present the sensor has frozen and measuring the same quantity at all time instances. A frozen sensor fault can be modeled as

$$y_{meas} = c, \forall t \quad (2.4)$$

For some constant c . A special case of frozen sensor fault is referred to as a dead sensor fault, which occurs when $c = 0$.

It is desirable for the MBDS to be able to detect and isolate all the above listed sensor faults. In this thesis the task of detecting all kinds of sensor faults and isolating the defective sensor will be handled. The task of isolating what kind of sensor fault that is present will not be handled, for example, there will be no effort in categorizing a detected fault as a bias fault or a gain fault. The MBDS is also delimited to handle the occurrence of single faults in the system. Hence the task of isolating multiple faults will not be in the scope of this thesis.

Two different sets of fault modes for sensor faults will be considered, denoted the augmented set and the minimal set. The augmented set of fault modes are obtained by assuming that each fault can occur in each of the individual axes on the multi-axis sensors. Thus the three-axis sensors can generate proper measurements along two axes while a fault is present at the third. By assuming the opposite, i.e., that a sensor fault affects all axes of the sensor, the minimal set of fault modes is obtained. The set of fault modes is listed in Table 2.1 and 2.2.

Fault mode	Description
NF	No fault.
F _{mag}	Fault in the magnetometer.
F _{acc}	Fault in the accelerometer.
F _{gyro}	Fault in the gyroscope.
F _{GPS}	Fault in the GPS.
F _{stag}	Fault in the stagnation pressure sensor.
F _{stat}	Fault in the static pressure sensor.

Table 2.1: Minimal set of fault modes in the model based diagnosis system, obtained by assuming that a sensor fault affects all axes of the sensor.

Fault mode	Description
NF	No fault.
F_{magX}	Fault in the X-axis of the magnetometer .
F_{magY}	Fault in the Y-axis of the magnetometer.
F_{magZ}	Fault in the Z-axis of the magnetometer.
F_{accX}	Fault in the X-axis of the accelerometer.
F_{accY}	Fault in the Y-axis of the accelerometer.
F_{accZ}	Fault in the Z-axis of the accelerometer.
F_{gyroX}	Fault in the X-axis of the gyroscope.
F_{gyroY}	Fault in the Y-axis of the gyroscope.
F_{gyroZ}	Fault in the Z-axis of the gyroscope.
F_{GPSalt}	Fault in the altitude indicated by the GPS.
F_{GPSlat}	Fault in the latitude indicated by the GPS.
F_{GPSlong}	Fault in the longitude indicated by the GPS.
$F_{\text{GPScourse}}$	Fault in the course indicated by the GPS.
F_{GPSspeed}	Fault in the speed indicated by the GPS.
F_{stag}	Fault in the stagnation pressure sensor.
F_{stat}	Fault in the static pressure sensor.

Table 2.2: Augmented set of fault modes in the model based diagnosis system, obtained by assuming that sensor faults only affects individual axes of the sensor.

2.4 Diagnosis Tests

A diagnosis test δ_i consists of a residual generator and a rejection region. The residual generator is a function from the measurements and states to a scalar value which is to be processed and thresholded by a threshold J_k . The output of a diagnosis test is a sub statement S_i , which contains information about which fault modes that can explain the behavior of the system. The structure of a diagnosis test is shown in Figure 2.3.



Figure 2.3: The structure of a diagnosis test

Each diagnosis test is sensitive to a certain set of faults. The set of tests that is performed in the autopilot defines fault detectability and isolability in the system, i.e. which faults that can be detected and which fault modes the system may be in. A structural algorithm for test design presented in Krysander et al. [2010] will be used to find test candidates. The algorithm is based on finding testable submodels from an overconstrained system of equations, called Test Equation Supports (TESs). Residual generation from the test candidates will be based on

linear transformations and the EKF, although other methods as Svard and Nyberg [2010] also would be interesting to apply.

2.4.1 Structural Analysis

In fault diagnosis, structural methods can be used to find testable set of equations in a model. Many structural algorithms, such as Krysander et al. [2008] are based on finding Minimal Structurally Overconstrained (MSO) sets of equations, which are minimal sets of equations containing redundancy. The number of MSO-sets grows exponentially in the degree of redundancy in the model. Hence, the task of computing all MSO sets and designing residuals for each of them becomes difficult for systems with high degree of redundancy, like the UAV system.

In difference to algorithms based on finding MSO sets, the TES concept takes the influence of faults into account to find a smaller number of testable systems of equations. The concept of TES and a closely related concept called Test Support (TS) will be explained and formally defined in the following subsection.

Definitions

In order to introduce the concept of TES and the algorithm for finding all TESs, some definitions needs to be stated. In the definitions, the set of equations that form the model is denoted M . According to Krysander et al. [2010] the concept of a Proper Structurally Overdetermined (PSO) set of equations, TES, TS, minimal TES (MTES), and minimal TS (MTS) is defined as

2.3 Definition. *A set of equations M is proper structurally overdetermined (PSO) if $M = M^+$ and minimally structurally overdetermined (MSO) if no proper subset of M is overdetermined. Where M^+ is a overdetermined system of equations, i.e. M^+ contains more equations than variables.*

2.4 Definition. *Given a model \tilde{M} and a set of faults \tilde{F} , a subset of faults $\zeta \subseteq \tilde{F}$ is a TS if there exists a PSO set $M \subseteq \tilde{M}$ such that $F(M) = \zeta$. Where $F(M)$ represents the set of faults that affects any of the equations in the model M .*

2.5 Definition. *Given a model, a TS is a minimal TS (MTS) if no proper subset is a TS.*

2.6 Definition. *An equation set M is a Test Equation Support (TES) if*

1. $F(M) \neq \mathbf{NF}$
2. M is a PSO set, and
3. for any $M' \supsetneq M$ where M' is a PSO set it holds that $F(M') \supsetneq F(M)$.

2.7 Definition. *A TES M is a minimal TES (MTES) if there exists no subset of M that is a TES.*

A TS (or MTS) can be interpreted as a set of faults that affects a test. A TES (or MTES) is a set of equations that can be used to form a test with corresponding fault sensitivity. A TS ζ and a TES M is related as

$$F(M) = \zeta \quad (2.5)$$

(Minimal) Test Equation Support Algorithm

The concepts of TS and TES are of high importance when designing tests and performing isolability analysis. In Krysander et al. [2010] efficient algorithms for finding all TESs and MTESs in a non-linear model are presented. The algorithms are recursive, in which one equation at the time is removed from the overdetermined part of the model and the overdetermined part of the remaining model is computed. This corresponds to a depth-first search through the nodes.

In this thesis the algorithms will be applied to the non-linear UAV model in order to find all MTESs and TESs. When applying structural algorithms to a non-linear model, only best-case results are obtained. A structurally detectable fault might not be detectable in practice, since it might not be possible to compute a residual from the overdetermined part of the model. High amount of measurement noise or model uncertainties can also become practical issues. Hence, all TES and MTES generated by the algorithms will be seen as candidates from which it might be possible to design tests. A software packet with MATLAB implementation of the algorithms is provided in Krysander et al. [2010].

2.5 Fault Detection

In a perfect world, the residuals would be zero when no fault occur and non-zero when a fault occur. Due to measurement noise and process disturbances, this is not the case in real applications. In fault diagnosis, thresholding algorithms are used to detect faults in the system by processing of the residuals.

2.5.1 Thresholding

A threshold J defines the maximum tolerated deviation from zero for the residuals. If the absolute value of the residual exceeds the threshold, a fault is present. The threshold can be a constant or a function of some variables.

$$\begin{aligned} |r(t)| < J & \text{ No fault detected} \\ |r(t)| > J & \text{ Fault detected} \end{aligned} \quad (2.6)$$

2.5.2 Filtering

In order to reduce the amount of noise in the residuals and hence reduce the probability of false alarms, the residuals are often filtered before they are compared to a threshold. In filtering the following signal model is used

$$y(t) = \theta(t) + e(t) \quad (2.7)$$

where $y(t)$ is the measured signal which consists of a deterministic component $\theta(t)$, and additive white noise $e(t)$. The task of determining $\theta(t)$ from $y(t)$ is called estimation.

The standard approach in signal processing for separating the signal $\theta(t)$ and the noise $e(t)$ are by filtering (typically low-pass)

$$\hat{\theta}(t) = H(q)y(t) \quad (2.8)$$

where $H(q)$ is the transfer function of the filter. An alternative interpretation of filtering is data windowing

$$\hat{\theta}(t) = \sum_{k=0}^{\infty} w_k y(t-k) \quad (2.9)$$

where the weights should satisfy $\sum w_k = 1$. This is equal to filtering approach if the weights are interpreted as the impulse response of the filter. A fundamental principle is to use a sliding window defined by

$$w_k = \begin{cases} \frac{1}{L} & 0 \leq k < L \\ 0 & k \geq L \end{cases} \quad (2.10)$$

The sliding window is a Finite Impulse Response (FIR) filter.

2.5.3 Change Detection

Change detection is the task of finding abrupt or rapid changes in $\theta(t)$, according to Gustafsson [2000]. The change time is denoted k_a . An algorithm that is commonly used in change detection is the cumulative sum (CUSUM) test. The CUSUM test is used to give an alarm when $\theta(t)$ has exceeded a certain threshold. An auxiliary test statistic $g(t)$ is introduced, which is used for alarm decisions using a threshold h .

$$\text{Alarm if } g(t) > h \quad (2.11)$$

Equation (2.11) will be referred to as the stopping rule. The input to the stopping rule is a distance measure $s(t)$. The most common approach is to use the absolute value of the residuals as a distance measure

$$s(t) = |r(t)| \quad (2.12)$$

An alternative approach is to use the squared residuals

$$s(t) = r^2(t) \quad (2.13)$$

This is useful for detecting both variance and parameter changes. Equation (2.14) defines the CUSUM algorithm.

$$g(t) = \begin{cases} g(t-1) + s(t) - v & \text{if } g(t) < 0 \\ 0 & \text{if } g(t) > h > 0 \\ g(t-1) + s(t) - v, \text{ and } k_a = t & \text{if } g(t) > h > 0 \end{cases} \quad (2.14)$$

In the CUSUM algorithm the test statistic $g(t)$ sums up its input $s(t)$, with the idea to give an alarm when the sum exceeds a threshold h . With white noise as input, the test statistic will drift away similar to a random walk. To prevent positive drift eventually yielding a false alarm, a small drift term v is subtracted at each time instant. To prevent a negative drift which would increase the time of detection, the test statistic is reset to zero if it becomes negative.

2.6 Decision Logic

The decision logic decides which fault modes that can explain the behavior of the system given the diagnosis sub statements S_i from the individual tests. A diagnosis sub statement is a subspace of the set of fault modes Θ , i.e.:

$$S_i \in \{\mathbf{NF}, \mathbf{F}_{\text{mag}}, \mathbf{F}_{\text{acc}}, \mathbf{F}_{\text{GPS}}, \mathbf{F}_{\text{stag}}, \mathbf{F}_{\text{stat}}\} \quad (2.15)$$

If the minimal set of fault modes is used. The diagnosis statement S is determined as

$$S = S_1 \cap S_2 \cap \dots \cap S_N \quad (2.16)$$

where N is the number of diagnosis sub statements, which equals the number of tests. The principle of generating an alarm can be expressed as

$$\begin{array}{ll} \mathbf{NF} \in S & \text{NOT generate an alarm} \\ \mathbf{NF} \notin S & \text{Generate an alarm} \end{array}$$

If the fault free mode \mathbf{NF} can explain the behavior of the system there is no reason

to generate an alarm. If **NF** is not contained in the diagnosis statement the system should generate an alarm.

3

Coordinate Systems

This chapter describes the coordinate frames that are relevant for avionic navigation. The fundamentals of avionic navigation is described in Kayton and Fried [1997]. A survey of coordinate systems for attitude estimation for UAVs are done in previous theses at ICS, see Veiback [2010] and Magnusson [2013].

3.1 Earth-centered and Earth-fixed

A basic coordinate frame for navigation near the earth is the Earth-Centered, Earth-Fixed (ECEF). The ECEF is a Cartesian coordinate system (X^E, Y^E, Z^E) , whose origin is at the mass center of the earth. The ECEF system rotates with the earth and the axes are fixed with respect to the earth as shown in figure 3.1. The (Z^E) -axis is aligned with the north pole of the earth and the (X^E) -axis is aligned with Greenwich Prime. The (Y^E) -axis is defined such that a right hand system is achieved.

A position on the earth is often described using a World Geodetic System (WGS). In the WGS a position on the earth is defined by longitude, latitude and height over sea level. Longitude (λ) is the angle between the Greenwich median and the position. Latitude (ϕ) is the angle between the equatorial plane and the position. The earth is modeled as a rotationally symmetric ellipsoid with the origin at the mass center of the earth. The international standard is called the World Geodetic System with the latest revision in 1984, (WGS84). The WGS84 is defined in Imagery and Agency [2000]. The parameters defining the reference surface of the earth in WGS84 are described in Table 3.1.

The conversion from longitude-latitude and height over sea level to ECEF Cartesian coordinates is described in Magnusson [2013].

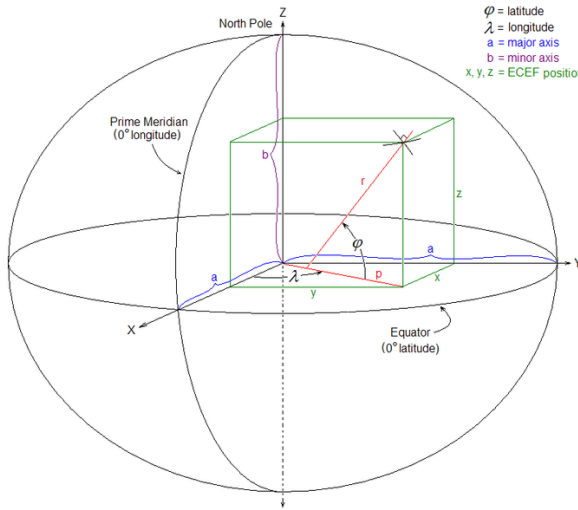


Figure 3.1: The Earth-centered, Earth-fixed coordinate frame

Description	Parameter	Value
Major radius	a	6378137 [m]
Minor radius	b	6356752.3142 [m]
Flattening	f	1/298.257223563
First eccentricity	e_1	$\sqrt{1 - \frac{b^2}{a^2}}$
Second eccentricity	e_2	$\sqrt{\frac{a^2}{b^2} - 1}$
IERS reference meridian	-	102.5[m] east of the Greenwich Prime.

Table 3.1: Parameters defining the reference for WGS84.

3.2 Local Geodetic Frame

A Local Geodetic Frame (LGF) is a coordinate system that is local in respect to a point somewhere over the Earth's surface. LGF is often used as navigation frame for aircrafts, fixed in the aircraft center of mass. Two axes span a tangential plane to the surface of the Earth and the third axis is orthogonal to this plane. In avionics the North-East-Down (NED)- frame is commonly used. The NED-frame is right-handed with the north component aligned with the geographical north pole. The down component is aligned with the local gravity vector and the east component defined as east relative to the geographical north pole. Figure 3.2 illustrates the local NED frame relative to the ECEF frame.

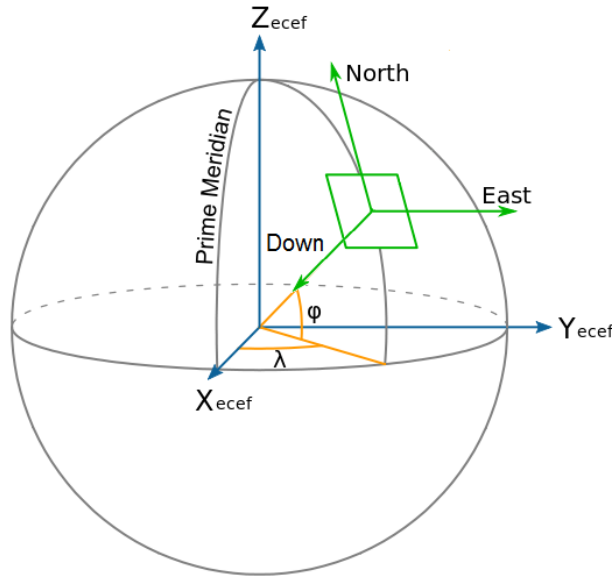


Figure 3.2: The Local North-East-Down coordinate frame

3.3 Body Frame

The body frame is fixed to the aircraft's center of mass. The axes are defined as:

X - Straight forward through the nose of the aircraft.

Y - Right of the aircraft.

Z - Down of the aircraft.

The orientation of the aircraft can be defined as the orientation of the body-frame with respect to a local geodetic frame. The orientation of the aircraft is often expressed in terms of the avionic angles (ψ), pitch (θ), and roll (ϕ). The rotation rates define the motion of the aircraft. The body frame and the avionic angles are illustrated in Figure 3.3.

3.4 Rotation Between Frames

In an autopilot system the GPS, magnetometers, accelerometers, gyroscopes, and barometers are used to estimate position, heading, and attitude. To be able to fuse measurements, a transformation between the different coordinate systems is necessary. Some measurements or states must be rotated into another coordinate system. There are several ways to represent a 3 dimensional rotation between two coordinate systems. Different algorithms are presented and evaluated in Shuster [1993]. The three most common methods to represent this rotation are:

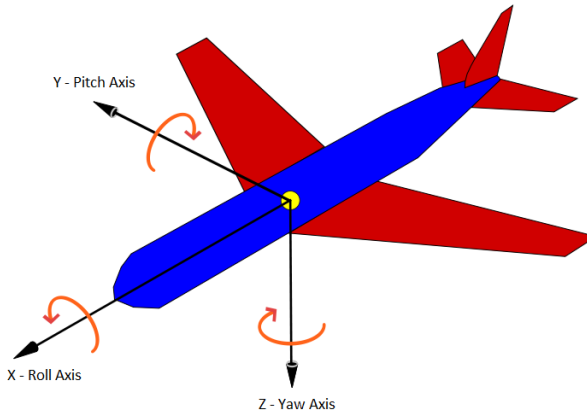


Figure 3.3: The Body frame

Euler angles - Euler angles represents the rotation between frames with three serial rotations around single axes. This is an intuitive way of rotating between frames but it contains a singularity for 90 degrees pitch.

Direction cosine matrix - Direction cosine matrix represents the rotation from one frame into another with a matrix multiplication. This method has no singularities but nine values to keep track of.

Quaternions - Using quaternions, the rotation between frames is performed as a single rotation is performed around an imaginary vector. This method has no singularities and only four states.

In the thesis the quaternions are used to represent rotations between frames. The quaternion representation is a natural choice in navigation, since it does not suffer from any weakness as the Euler angles. The only disadvantage is the lack of intuitive interpretation of a quaternion. The same notation as in Törnqvist [2006], Appendix B is used in this thesis.

3.4.1 Quaternions

The theory of quaternions were invented by Hamilton [1843]. In mathematics, quaternions are a number system that extends the complex numbers. The quaternion approach of the three dimensional rotation is to rotate a three dimensional space into another around a four dimensional vector which is orthogonal to the three dimensional spaces.

A quaternion is defined as

$$\mathbf{q} = q_0 + q_1\mathbf{i} + q_2\mathbf{j} + q_3\mathbf{k} = \begin{bmatrix} q_0 & q_1 & q_2 & q_3 \end{bmatrix} \begin{bmatrix} 1 \\ \mathbf{i} \\ \mathbf{j} \\ \mathbf{k} \end{bmatrix} \quad (3.1)$$

where \mathbf{i} , \mathbf{j} , and \mathbf{k} are imaginary components. A feature of quaternions is that the product of two quaternions is non commutative. The multiplication between quaternions is defined by

$$\begin{aligned} \mathbf{i} \cdot \mathbf{i} &= -1 & \mathbf{i} \cdot \mathbf{j} &= \mathbf{k} & \mathbf{i} \cdot \mathbf{k} &= -\mathbf{j} \\ \mathbf{j} \cdot \mathbf{j} &= -1 & \mathbf{j} \cdot \mathbf{i} &= -\mathbf{k} & \mathbf{j} \cdot \mathbf{k} &= \mathbf{i} \\ \mathbf{k} \cdot \mathbf{k} &= -1 & \mathbf{k} \cdot \mathbf{i} &= \mathbf{j} & \mathbf{k} \cdot \mathbf{j} &= -\mathbf{i} \end{aligned} \quad (3.2)$$

The multiplication between two arbitrary quaternions is given by

$$\begin{aligned} \mathbf{q} \cdot \mathbf{p} &= (q_0 + q_1\mathbf{i} + q_2\mathbf{j} + q_3\mathbf{k}) \cdot (p_0 + p_1\mathbf{i} + p_2\mathbf{j} + p_3\mathbf{k}) \\ &= (q_0p_0 - q_1p_1 - q_2p_2 - q_3p_3) + (q_0p_1 + q_1p_0 + q_2p_3 - q_3p_2)\mathbf{i} \\ &\quad + (q_0p_2 - q_1p_3 + q_2p_0 + q_3 + p_1)\mathbf{j} + (q_0p_3 + q_1p_2 - q_2p_1 + q_3p_0)\mathbf{k} \\ &= \begin{bmatrix} q_0 & -q_1 & -q_2 & -q_3 \\ q_1 & q_0 & -q_3 & q_2 \\ q_2 & q_3 & q_0 & -q_1 \\ q_3 & -q_2 & q_1 & q_0 \end{bmatrix} \begin{bmatrix} p_0 \\ p_1 \\ p_2 \\ p_3 \end{bmatrix} \end{aligned} \quad (3.3)$$

An alternative representation of the quaternion is

$$\mathbf{q} = \begin{bmatrix} q_0 \\ \mathbf{q} \end{bmatrix} \quad (3.4)$$

Where q_0 is a scalar and \mathbf{q} is a three dimensional vector. In order to express a vector $\mathbf{n}_A = [n_x \ n_y \ n_z]^T$ given in a frame \mathcal{A} into another frame \mathcal{B} , the components are redefined as the complex components of a quaternion,

$$\mathbf{q}_A = 0 + \mathbf{i}n_x + \mathbf{j}n_y + \mathbf{k}n_z \quad (3.5)$$

where \mathbf{q}_A is the quaternion in frame \mathcal{A} . The real valued component is set to zero. The rotation from frame \mathcal{A} to frame \mathcal{B} is defined as

$$\mathbf{q}_B = \mathbf{q}^* \mathbf{q}_A \mathbf{q} \quad (3.6)$$

For some quaternion $\mathbf{q} = q_0 + q_1\mathbf{i} + q_2\mathbf{j} + q_3\mathbf{k}$. Where \mathbf{q}_B is the corresponding quaternion in frame \mathcal{B} . \mathbf{q}^* denotes the complex conjugate of \mathbf{q} and is defined as a negation of all the complex components, which is the same as the inverse of the quaternion. Expanding (3.6) using the multiplication formula (3.2), gives the relationship between the vector in the different reference frames

$$\mathbf{q}_B = \begin{bmatrix} 0 & 0 & 0 & 0 \\ 0 & q_0^2 + q_1^2 - q_2^2 - q_3^2 & 2(q_1q_2 + q_0q_3) & 2(q_1q_3 - q_0q_2) \\ 0 & 2(q_1q_2 - q_0q_3) & q_0^2 - q_1^2 + q_2^2 - q_3^2 & 2(q_2q_3 + q_0q_1) \\ 0 & 2(q_1q_3 + q_0q_2) & 2(q_2q_3 - q_0q_1) & q_0^2 - q_1^2 - q_2^2 + q_3^2 \end{bmatrix} \mathbf{q}_A \quad (3.7)$$

The rotation is given by a 4 by 4 matrix that contain only zeros in its first row and column. Note that \mathbf{q}_A and \mathbf{q}_B is quaternions defined by equation (3.5). Equation (3.7) can be interpreted as a 3 by 3 rotation matrix, equivalent to the direction cosine matrix described in Shuster [1993]. The rotation matrix is defined by the components of the quaternion \mathbf{q} , according to Equation (3.8).

$$R(\mathbf{q}) = \begin{bmatrix} q_0^2 + q_1^2 - q_2^2 - q_3^2 & 2(q_1q_2 + q_0q_3) & 2(q_1q_3 - q_0q_2) \\ 2(q_1q_2 - q_0q_3) & q_0^2 - q_1^2 + q_2^2 - q_3^2 & 2(q_2q_3 + q_0q_1) \\ 2(q_1q_3 + q_0q_2) & 2(q_2q_3 - q_0q_1) & q_0^2 - q_1^2 - q_2^2 + q_3^2 \end{bmatrix} \quad (3.8)$$

The direction cosine matrix is defined in the avionic angles yaw (ψ), pitch (θ), and roll (ϕ).

$$R_{\cos}(\psi, \theta, \phi) = \begin{bmatrix} \cos \theta \cos \psi & \cos \theta \sin \psi & -\sin \theta \\ \sin \phi \sin \theta \cos \psi & \sin \phi \sin \theta \sin \psi & \sin \phi \cos \theta \\ -\cos \phi \sin \psi & +\cos \phi \cos \psi & \\ \cos \phi \sin \theta \cos \psi & \cos \phi \sin \theta \sin \psi & \cos \phi \cos \theta \\ +\sin \phi \sin \psi & -\sin \phi \sin \psi & \end{bmatrix} \quad (3.9)$$

Since the rotation matrix $R(\mathbf{q})$ must be equivalent to the direction cosine matrix $R_{\cos}(\psi, \theta, \phi)$, the avionic angles can be expressed in the components of the quaternion \mathbf{q} by element wise identification. The following identities holds.

$$\psi = \arctan \left(\frac{R(\mathbf{q})^{12}}{R(\mathbf{q})^{11}} \right) = \arctan \left(\frac{2(q_1q_2 + q_0q_3)}{q_0^2 + q_1^2 - q_2^2 - q_3^2} \right) \quad (3.10)$$

$$\theta = -\arcsin \left(R(\mathbf{q})^{13} \right) = \arcsin (2(q_1q_3 - q_0q_2)) \quad (3.11)$$

$$\phi = \arctan \left(\frac{R(\mathbf{q})^{23}}{R(\mathbf{q})^{33}} \right) = \arctan \left(\frac{2(q_2 q_3 + q_0 q_1)}{q_0^2 - q_1^2 - q_2^2 + q_3^2} \right) \quad (3.12)$$

For a moving body-system, the rotations between a fixed reference system and a body reference system will contain dynamics. The time derivative of the quaternion can be calculated as

$$\dot{\mathbf{q}} = \frac{1}{2} S(\boldsymbol{\omega}) \mathbf{q} = \frac{1}{2} \bar{S}(\mathbf{q}) \boldsymbol{\omega} \quad (3.13)$$

where

$$S(\boldsymbol{\omega}) = \begin{pmatrix} 0 & -\omega_x & -\omega_y & -\omega_z \\ \omega_x & 0 & \omega_z & -\omega_y \\ \omega_y & -\omega_z & 0 & \omega_x \\ \omega_z & \omega_y & -\omega_x & 0 \end{pmatrix} \quad (3.14)$$

$$\bar{S}(\mathbf{q}) = \begin{pmatrix} -q_1 & -q_2 & -q_3 \\ q_0 & -q_3 & q_2 \\ q_3 & q_0 & -q_1 \\ -q_2 & q_1 & q_0 \end{pmatrix} \quad (3.15)$$

where \mathbf{q} is the quaternion that defines the rotation between the fixed reference system and the body reference system.

4

Sensors

This chapter is intended as an analysis of the sensors on the EasyPilot and their performance. The content of this chapter is the result of previous master theses done on the behalf for ICS, Magnusson [2013] and Veiback [2010]. The sensors on EasyPilot belong to the Micro-Electro-Mechanical System (MEMS) technology. The Sensor Unit (SU) consists of small sensor elements, in the range 0.02 to 1 mm, together with a processing unit.

4.1 Gyroscopes

A MEMS gyroscope measures rotational rate around a fix axis. The EasyPilot is equipped with a 3-axis analog MEMS gyroscope. Gyroscopes can be integrated to acquire orientation of the aircraft. The rotation rates can also be used to suppress external disturbances. The gyroscopes are sampled by the processor at approximately 200 Hz.

4.1.1 Performance

When using a MEMS gyroscope there are several factors and error sources to take into account, as described in Jay Esfandyari [2010]. The following error sources are important to be aware of:

Bias - If the sensor is laying still and not has zero mean on all axis, a bias is present.

Alignment errors - The axes of the sensors can be non-orthogonal. If the aircraft rotates around one of its own axes, another axes will indicate a rotation as well.

Scale factor - Since the gyroscopes are analog sensors, the measured voltage from the sensor must be converted into rotation rate. This conversion is done using a scale factor, which in general is given by the manufacturer.

Non-linearity - The scaling factor is not necessary a constant. It may differ between different rotation rates. The scale factor may also depend on temperatures and accelerations.

Bias and scaling stability - The bias and scale factor may differ over time.

These types of errors can be compensated for by proper calibration of the gyroscope. During the master thesis, the calibration algorithm in Magnusson [2013] will be used. Hence, only bias and constant scaling factor errors will be compensated for. Other sensor specific performance factors such as resolution, bandwidth, turn-on time, and shock resistance will not be taken into account due to lack of reliable measurement tools.

4.1.2 Statistical Analysis

Most information about the gyroscope can be gathered by collecting data when the sensor is placed at standstill. In this section bias and noise levels will be presented. Using a logged dataset, bias and variance could be derived. Due to limitations in the communication between the EasyPilot and the Ground Control Station (GCS), the gyros are sampled at approximately 120Hz. The bias and the variance of this dataset is presented in Table 4.1.

Axis	Bias [rad/s]	Variance [rad ² /s ²]
X	-0.1069	$2.84e^{-4}$
Y	-0.1268	$5.65e^{-4}$
Z	-0.0192	$5.66e^{-5}$

Table 4.1: Gyroscope bias and variance.

The EasyPilot is not an ideal mounting position of the gyroscopes since lots of electronic components, causing local electronic disturbances in power supply and inducing currents in the gyroscope circuit which affects the measurements.

4.1.3 Calibration

The gyroscopes are calibrated for bias and constant scaling. The output voltage from the gyroscope is transformed into angular rate according to

$$\omega = (U - b^U) \cdot k \quad (4.1)$$

where b^U is the bias and k is the scale factor. The bias is identified by sampling the gyroscopes while lying still. In order to get a good calibration of the scaling factor, a precise known rotation around a single axis is needed.

4.2 Accelerometers

An accelerometer measures proper acceleration (which is weight per unit of a test mass). The actual gravity of the earth and accelerations due to motion is measured by the accelerometer. Theoretically both velocity and position can be estimated by integration of the measurements from the accelerometer. The accelerometer can also be used to estimate the orientation, since the reference gravity vector is known in the NED frame. The accelerometer used in EasyPilot is an analog 3-axis MEMS accelerometer.

4.2.1 Performance

The performance of the accelerometers can be evaluated in roughly the same manner as the gyroscopes. Since both the accelerometers and gyroscopes are MEMS technology they will have the same errors related to the MEMS technology. The accelerometer can be used to gain long-term stability in orientation. In navigation, only short-term stability can be achieved since the position is a double integration. For strapdown systems this is further discussed in Titterton et al. [2004], and is also discussed more general in Gustafsson [2010].

4.2.2 Stastical Analysis

Most information about the accelerometer can be gathered by collecting data when the sensor is placed at standstill and flat orientated, which means that the z-axis should align with the negative gravity vector. Hence, the z-axis accelerometer should measure one negative g. Using a logged dataset, bias and variance can be derived. The accelerometers is sampled at approximately 120 Hz. The bias and the variance of this dataset is presented in Table 4.2.

Accelerometer	Bias [g]	Variance [$\mu\text{g}/\sqrt{\text{Hz}}$]
X	-0.0475	193.92
Y	0.0562	207.62
Z	-0.0406	454.60

Table 4.2: Accelerometer bias and variance.

When performing measurements for estimation of accelerometer bias the orientation of the sensor is of extreme importance. A tilted sensor will cause that accelerometers that should be orthogonal to the gravity vector measures part of the gravity vector. This must not be interpreted as sensor bias. The accelerometers also suffers from the same electronic disturbances as discussed in section 4.1.2.

4.2.3 Calibration

In this master thesis, the calibration algorithm in Magnusson [2013] will be used. This algorithms compensates for scale factors and biases on the individual axes. An algorithm for calibrating the accelerometer with respect to misalignment is presented in Spectrum and Inc [2010].

4.3 Magnetometer

A magnetometer is used to measure the strength and the direction of magnetic fields. The EasyPilot is equipped with a tri-axis anisotropic magnetoresistive (AMR) magnetometer. This kind of magnetometer is often used in strapdown applications. In avionic applications the magnetometer is often used to determine the heading of the aircraft. The orientation of the aircraft can be determined by measuring the strength and direction of the earth's magnetic field, which is known.

4.3.1 Performance

When using a magnetometer to determine the heading of the aircraft, there are several factors and error sources to take into account. The following error sources are important to be aware of

Disturbance fields - The field strength of the earth's magnetic field is small, from $30 \mu T$ in South Africa, to $60 \mu T$ at the poles. Disturbance fields generated by electric motors and high voltage wires will also be measured by the sensor. On the EasyPilot lots of electronics components will disturb the magnetometer. Figure 4.1 shows the calibrated measurements from the magnetometer while the motor of the aircraft generates a disturbance field.

The geographical position - The geographical position where the magnetometer is used is of great importance. The angle between the surface and the magnetic field increases when as the distance to the magnetic pole decreases. This is called inclination or dip.

Deviation from geographical north - The magnetic north pole deviates from the geographical north pole. The angle between the magnetic north component and the geographical north component is called the declination.

In Linköping the declination is approximately 4° and the inclination 70° . Hence, the magnetic component in the horizontal plane is small relative to its component in the vertical plane. A small magnetic component in the horizontal plane means that the heading estimate from the magnetometer will be less accurate. In the NED frame the earth's magnetic field can be separated into three components. In Linköping these are given by:

Component	Value [μT]
North	15.741
East	1.1304
Down	48.422

Table 4.3: Field strength of the magnetic field in Linköping, North-East-Down frame

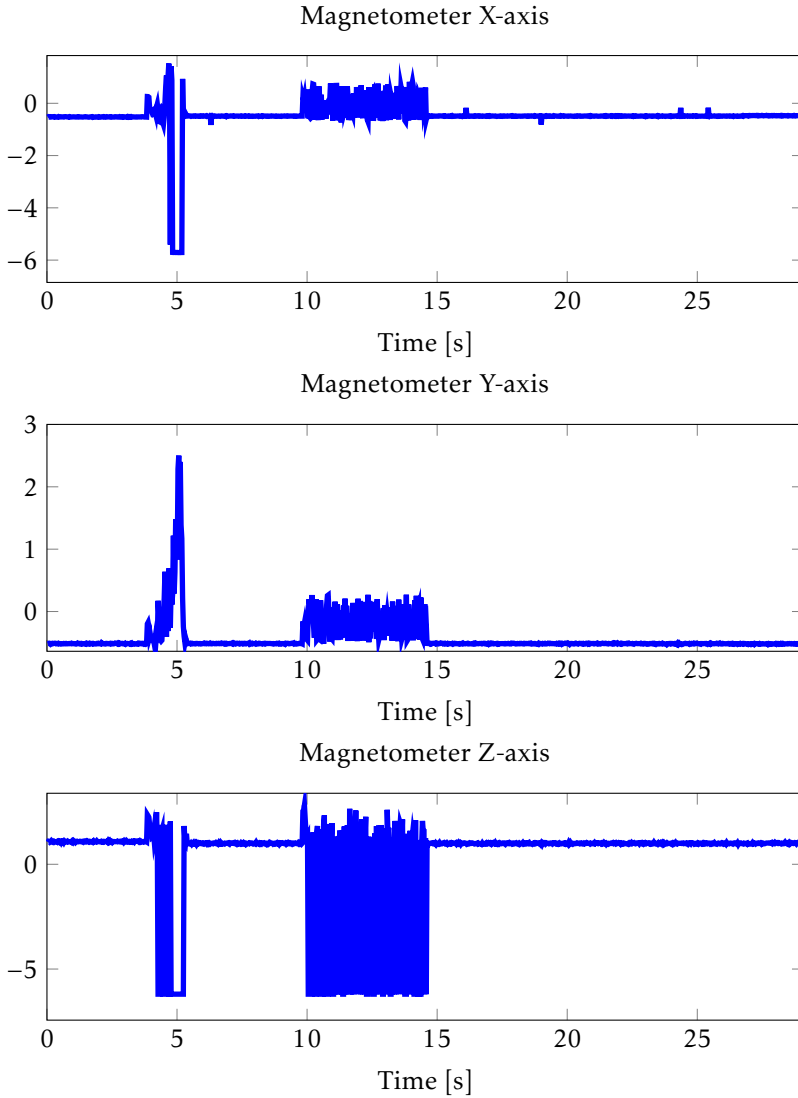


Figure 4.1: Calibrated magnetometer measurements. The engine of the aircraft introduces hard iron perturbations.

4.3.2 Calibration

The magnetometer should be calibrated to compensate for errors as alignment errors, element sensitivity errors, element magnetization errors, hard iron errors, and soft iron errors. The error sources, as well as the calibration algorithm is further discussed in Magnusson [2013]. Due to the soft and hard iron errors the calibration must be done when the sensor is mounted on the aircraft.

If only measurement noise is modeled the model would be

$$\hat{\mathbf{h}} = \mathbf{h}_s + \epsilon \quad (4.2)$$

where $\hat{\mathbf{h}}$ is the measured magnetic field, \mathbf{h}_s is the indicated magnetic field by the sensor, and ϵ is measurement noise. The hard iron effects can be compensated for using a bias term

$$\mathbf{b}_{\text{hi}} = [b_{hi_x} \ b_{hi_y} \ b_{hi_z}]^T. \quad (4.3)$$

The soft iron effects can be modeled as a scaling of the true magnetic field with a 3 by 3 matrix

$$\mathbf{A}_{\text{si}} = \begin{bmatrix} a_{11} & a_{12} & a_{13} \\ a_{21} & a_{22} & a_{23} \\ a_{31} & a_{32} & a_{33} \end{bmatrix} \quad (4.4)$$

hence, the sensor is actually measuring

$$\mathbf{h} = \mathbf{A}_{\text{si}}(\mathbf{h}_s - \mathbf{b}_{\text{hi}}) \quad (4.5)$$

In order to compensate for the measurement errors in the sensor, the Wheatstone bridge misalignments and the scaling of the current magnetic field must be compensated for. The misalignments can be compensated for by multiplying the measurement with a 3 by 3 matrix on the orthogonal frame in which the sensor is mounted. The scaling of the current magnetic field can be compensated for by multiplying with a 3 by 3 scaling matrix, which is a diagonal matrix. The bias in the sensor is compensated for by subtract it for the measurement.

$$\mathbf{M} = \begin{bmatrix} m_{11} & m_{12} & m_{13} \\ m_{21} & m_{22} & m_{23} \\ m_{31} & m_{32} & m_{33} \end{bmatrix} \quad \text{non-orthogonality compensation}$$

$$\mathbf{S} = \begin{bmatrix} s_{11} & 0 & 0 \\ 0 & s_{22} & 0 \\ 0 & 0 & s_{33} \end{bmatrix} \quad \text{scaling compensation}$$

$$\mathbf{b}_s = [b_{s_x} \ b_{s_y} \ b_{s_z}]^T \quad \text{sensor bias compensation}$$

this yields the complete measurement equation

$$\hat{\mathbf{h}} = \mathbf{SM}(\mathbf{A}_{\text{si}}\mathbf{h}_e + \mathbf{b}_{\text{hi}}) + \mathbf{b}_s + \epsilon \quad (4.6)$$

In this thesis there is no interest in the individual contributions from the specific

error, hence the measurement equations can be expressed as

$$\hat{\mathbf{h}} = \mathbf{A}\mathbf{h}_e + \mathbf{b} + \boldsymbol{\epsilon} \quad (4.7)$$

with

$$\mathbf{A} = \mathbf{SMA}_{si} \quad (4.8)$$

$$\mathbf{b} = \mathbf{SMb}_{hi} + \mathbf{b}_s. \quad (4.9)$$

To be able to determine the orientation of the aircraft, equation (4.7) can be solved for \mathbf{h}_e

$$\mathbf{h}_e = \mathbf{A}^{-1}(\hat{\mathbf{h}} - \mathbf{b} - \boldsymbol{\epsilon}) \quad (4.10)$$

This calibration algorithm is used on the EasyPilot. The performance of this calibration is evaluated in Magnusson [2013]. Calibrated and uncalibrated measurements from the magnetometer is shown in Figure 4.2.

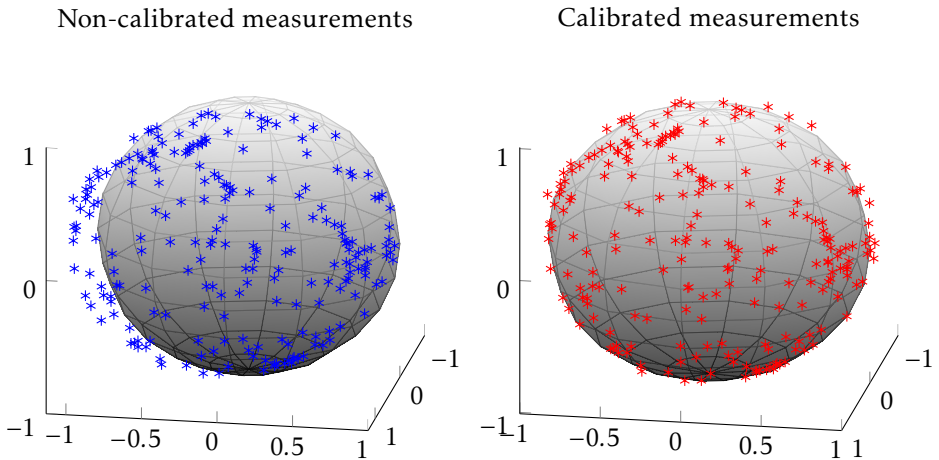


Figure 4.2: Uncalibrated and calibrated magnetometer measurements. The magnetometer is calibrated on a unit sphere. The right figure shows the normalized raw measurements and the left figure shows the calibrated measurements. It can be seen that the calibrated measurements fits better to the unit sphere.

4.4 Pressure Sensors

The EasyPilot is equipped with two pressure sensors. One sensor for measuring the static pressure and one sensor for measuring the stagnation pressure. The pressure sensor are MEMS technology. Stagnation pressure is defined by Bernoulli's equation.

$$P_{stagnation} = P_{static} + P_{dynamic} \quad (4.11)$$

Equation (4.11) can be solved for $P_{dynamic}$ since P_{static} is measured by the static pressure sensor. Hence, both the static and the dynamic pressure can be obtained. The static pressure can be used to determine the altitude of the aircraft, if the pressure at ground level is known. The dynamic pressure can be used to determine the air speed.

4.4.1 Performance

To be able to compensate for the bias in the pressure sensor, the exact pressure in the environment must be known. But since the air pressure is not constant, a more attractive option is the calibrate an offset in which the bias is included.

4.4.2 Calibration

The stagnation pressure and the static pressure should be equal when the aircraft is standing still on the ground and not wind is present. The calibration of the pressure sensors will only include a bias compensation, such that the stagnation pressure equals the static pressure when the aircraft is not moving.

4.5 Global Navigation Satellite System

The Global Navigation Satellite System (GNSS) is a navigation system based on satellites with global coverage such as GPS. Each satellite continually transmits messages that includes time of transmission and the position of the satellites.

The receiver uses these messages to determine the transit time of each message and computes the distance to each satellite. Each of these distances and satellites locations define a sphere. The receiver is on the surface of each of these spheres when the distances and the satellites locations are correct. When receiving messages from four or more satellites, the receiver can determine its position. The NMEA protocol is the standard protocol for GPS messages, which is supported by most manufacturers.

4.5.1 Position Estimation

If the receiver clock is synchronized with the satellite clock and the satellite emits its current time, the distance to the satellite can be determined. This algorithm is called Time Of Arrival (TOA). The difference in time of arrival and the timestamps on the received message is used to determine the distance to the satellite

$$d = c\Delta t \quad (4.12)$$

where c is the speed of light and Δt is the time difference between the timestamp in the message and the time the message was received. This means that the re-

ceiver must be on a sphere with radius d around the satellite. Assumed that the receiver is on the earth, the receiver must be at the intersection of this sphere and the earth, which is a circle. By adding another satellite, another circle on the earth is obtained. The intersection of these two circles is two points. A third satellite gives a third circle, which coincides with only one of the two possible points that were obtained by the two previous satellites. Hence, at least three satellites is needed to be able to determine the position of the receiver.

However, in most real application the receiver clock is not synchronized with the atom clocks on the satellites. This introduces an unknown variable in the problem since the receiver must apply the Time Difference Of Arrival (TDOA) algorithm. Since the transmitting satellites are synchronized, pairwise differences are formed from the timestamps of the received messages. Each pair of satellites gives a hyperbola, which the receiver must be on. To be able to solve this system of equations at least four satellite is needed. The TOA and TDOA algorithms is described in Gustafsson [2010]. Figure 4.3 illustrates the TDOA method using three transmitters.

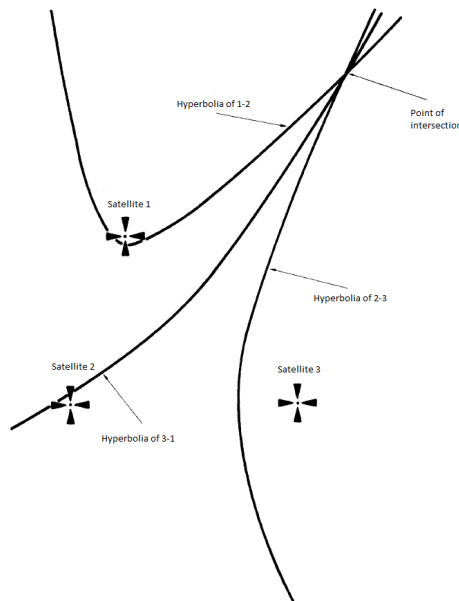


Figure 4.3: The TDOA method using three transmitters

4.5.2 Speed and Direction Estimation

Many receivers use extensive filtering from positioning to acquire speed estimate from the GPS. Modern receivers may track the frequency of the satellite signals and estimate the speed using the Doppler effect, see Chalko [2007].

5

Modeling

To be able to perform model based diagnosis, a mathematical model of the system is needed. To be able to relate measurements to information about the aircraft a measurement model is needed. As an example, the autopilot is equipped with a sensor to measure the static air pressure. The static air pressure is not interesting by itself, but together with a mathematical model the air pressure can be related to the altitude of the aircraft. The modeling of the aircraft and the EasyPilot is partly done in Magnusson [2013] and Veiback [2010]. In this section all measurement equations in the UAV system are derived. The complete model is summarized in Section 5.5.

A simple measurement model for a gyroscope that measures the angular velocity in rad/s , is to relate the measurement from the gyroscope to $^\circ/s$ as

$$y = \frac{\pi}{180} \omega \quad (5.1)$$

where ω is the measurement given in rad/s by the gyroscope and y is the angular velocity given in $^\circ/s$. A more complex measurement model that converts the angular velocity given by the gyroscope to an angle measured in rad can be stated as

$$\theta = \int \omega dt + \theta_0 \quad (5.2)$$

where ω is the measurement given in rad/s by the gyroscope, θ is the angle given in rad , and θ_0 is the angle at time $t = 0$. A more realistic model of the

gyroscope is that the sensor measures the angular velocity and some noise. The noise propagates through the measurement Equation (5.1) as

$$y = \frac{\pi}{180}(\omega + e) = \frac{\pi}{180}\omega + \frac{\pi}{180}e \quad (5.3)$$

where e is the measurement noise. As seen in (5.3) manipulation of the measured signal manipulates the measurement noise as well.

5.1 Attitude Estimation Model

This section contain measurement models to estimate the orientation of the aircraft in the NED-frame. In order to transform measurements between the body-frame and the NED-frame a rotation matrix as described in Section 3.4 is required. The orientation of the aircraft can be expressed in terms of the avionic angles yaw ψ , pitch θ , and roll ϕ , or using a rotation quaternion \mathbf{q} . Superscript b and N indicates that the signal is given in the body-frame or NED-frame respectively.

5.1.1 Accelerometers

The accelerometer measures acceleration in the body-frame. The accelerations measured by the sensor be summerized as

\mathbf{g}	The gravity of the earth
\mathbf{a}_t	Accelerations caused by the thrust
\mathbf{a}_c	Centripetal accelerations

where the sum of \mathbf{a}_t and \mathbf{a}_c is referred to as the external acceleration

$$\mathbf{a}_e = \mathbf{a}_t + \mathbf{a}_c \quad (5.4)$$

In order to compare the measurements from the accelerometer with the gravity vector given in the NED-frame, it must be transformed to the body-frame

$$\mathbf{y}_{\text{acc}}^b = R_n^b(\mathbf{g}) + \mathbf{a}_e^b \quad (5.5)$$

where $\mathbf{y}_{\text{acc}}^b$ is the measured accelerations and R_n^b is the rotation matrix from the NED-frame to the body-frame. The centripetal accelerations experienced in the body is derived in Euston et al. [2008] and can be estimated as

$$\mathbf{a}_c^b = \boldsymbol{\omega} \times (\boldsymbol{\omega} \times \rho \mathbf{r}) \quad (5.6)$$

where ω is the angular velocity, ρ is the curve radius, and \mathbf{r} is an unit vector pointing towards the center of the turn. By assuming that the angle of attack is close to zero, Equation (5.6) can be simplified according to

$$\mathbf{a}_c^b = \omega \times \begin{pmatrix} |v_a| \\ 0 \\ 0 \end{pmatrix} \quad (5.7)$$

where $|v_a|$ is the air speed, which is measured by the pressure sensors on the aircraft. The angular velocity ω is measured by the gyroscopes. The accelerations caused by the thrust are the accelerations that sets the aircraft in motion. These accelerations are equal to the derivate of the air speed with respect to time, which can be approximated using an Euler forward approximation

$$a_t^b = \frac{|v_{a,t}| - |v_{a,t-1}|}{T_s} \quad (5.8)$$

where T_s is the sample time of the sensor. Assuming that no other accelerations are affecting the body, the measurement Equation 5.5 becomes

$$\mathbf{y}_{acc}^b = R_b^n(\mathbf{g}) + \omega \times \begin{pmatrix} |v_a| \\ 0 \\ 0 \end{pmatrix} + \begin{pmatrix} a_t^b \\ 0 \\ 0 \end{pmatrix} \quad (5.9)$$

which can be used to estimate the rotation matrix R_b^n and thus the attitude of the aircraft can be determined.

5.1.2 Magnetometers

The measurements equation for the magnetometer is similar to the measurement equation for the accelerometer. The magnetometer measures a local magnetic field in the body-frame. As described in Section 4.3 the magnetic field of the earth is a known constant in the NED-frame, assuming that the aircraft don't travel over large distances. A measurement model of the magnetometer is given by

$$\mathbf{y}_{mag}^b = R_b^n \mathbf{B}^N \quad (5.10)$$

where \mathbf{y}_{mag} is the calibrated measurement. The measurement equation can be used in the same manner as Equation (5.9) to estimate the rotation matrix R_b^n and thus the attitude of the aircraft.

5.1.3 Gyroscopes

The gyroscope measures the rotational rate of the aircraft. The rotational rate is the angular velocity around the fixed axes of the aircraft. The rotation around the axes of the aircraft is denoted ω_x , ω_y , and ω_z . The measurement model to estimate the rotation rate from the gyroscopes can be expressed as

$$\mathbf{y}_{gyro} = \begin{pmatrix} \omega_x \\ \omega_y \\ \omega_z \end{pmatrix} \quad (5.11)$$

where \mathbf{y}_{gyro} is the calibrated gyroscope measurement. In Magnusson [2013] the gyroscope biases are treated explicitly in the measurement equation since the biases may vary over time. This approach gives the possibility to use estimate the gyroscope biases using a filter. Such a measurement model can be expressed as

$$\mathbf{y}_{gyro} = \begin{pmatrix} \omega_x \\ \omega_y \\ \omega_z \end{pmatrix} + \begin{pmatrix} b_{gyro,x} \\ b_{gyro,y} \\ b_{gyro,z} \end{pmatrix} \quad (5.12)$$

where \mathbf{y}_{gyro} is the measurement from the gyroscope and $b_{gyro,x}$, $b_{gyro,y}$, and $b_{gyro,z}$ are the gyroscope biases. A measurement model for estimating the attitude of the aircraft in the NED-frame, from the gyroscope can be obtained by integration of the measurements

$$\begin{pmatrix} \psi \\ \theta \\ \phi \end{pmatrix} = \int R_b^n \begin{pmatrix} \omega_x \\ \omega_y \\ \omega_z \end{pmatrix} dt + \begin{pmatrix} \psi_0 \\ \theta_0 \\ \phi_0 \end{pmatrix} \quad (5.13)$$

where ψ_0 , θ_0 , and ϕ_0 is the initial attitude of the aircraft. The rotation matrix R_b^n transforms the measurements from the body-frame to the NED-frame. However, since model contain integration of the measurements the estimate will suffer from integration drift.

5.1.4 GPS

A measurement model to estimate the yaw angle or heading ψ from the GPS is given by

$$\psi = \Psi_{GPS} \quad (5.14)$$

where Ψ_{GPS} is the course indicated by the GPS.

5.2 Height Estimation Model

This section describes measurement models to estimate the height over sea level.

5.2.1 GPS

A measurement model to estimate the height over sea level from the GPS can be derived as

$$h = h_{GPS} \quad (5.15)$$

where h_{GPS} is the height indicated from the GPS.

5.2.2 Static Pressure Sensor

A virtual measurement model for measuring height over sea level from static pressure is derived in Veiback [2010], according to

$$h = K \log\left(\frac{P_{s0}}{P_s}\right) + h_0 \quad (5.16)$$

where P_s is the measured static pressure, h_0 is the height (over sea level) at ground level, P_{s0} is the static pressure at ground level, and K is a constant that depends on temperature. To be able to use this measurement model the constant parameters h_0 , P_{s0} , and K must be known. The task of estimate these parameters is referred to as calibration of the measurement model. The parameter h_0 is set to the indicated GPS height at ground level, and P_{s0} is set to the measured static pressure at ground level. Since the parameter K is dependent on temperature it can change over time. In Magnusson [2013] the parameter K is estimated on-line using the Recursive Least Square (RLS) algorithm, with the indicated GPS height as a reference. In a diagnosis application this approach contains a major drawback. A fault in the GPS will affect K and thereby affect the measurement model for the static pressure. With this issue in mind, the parameter K will be derived from the laws of physics assuming a constant air temperature.

$$K = \frac{RT}{gM} \quad (5.17)$$

where R is the gas constant, T is the temperature of the air measured in Kelvin, g is the gravity of the earth, and M is the molar mass of the air.

5.3 Velocity Estimation Model

This section describes measurement models to the velocity and speed of the aircraft, where the terms air speed and ground speed is used. The air velocity \mathbf{v}_a

and the ground velocity \mathbf{v}_g is given in the NED frame, they are related as

$$\mathbf{v}_g = \mathbf{v}_a + \mathbf{v}_w \quad (5.18)$$

where \mathbf{v}_w is the velocity of the air (the wind), given in the same reference frame as \mathbf{v}_a and \mathbf{v}_g . The speed is defined as the norm of the velocity vector of the aircraft.

5.3.1 Ground Speed

A measurement model to estimate the ground speed from the GPS can be derived as

$$|\mathbf{v}_g| = s_{GPS} \quad (5.19)$$

where s_{GPS} is the speed indicated by the GPS.

A measure model to estimate the ground velocity from the accelerometers can be derived as

$$\mathbf{v}_g = \int R_b^n(\mathbf{a} - \mathbf{g})dt + \mathbf{v}_0 \quad (5.20)$$

where R_b^n is a rotation matrix to transform the measurements from body-frame to NED-frame, \mathbf{g} is the gravity vector in the NED-frame, and \mathbf{v}_0 is the speed at time $t = 0$. Since the measurement model contains integration of the measurement the estimate will suffer from integration drift, further described in Luinge et al. [1999].

5.3.2 Air Speed

The air speed can be estimated from the dynamic pressure. The dynamic pressure p_{dyn} , defined in Section 4.4 can be derived from the measurements of the pressure sensors. A measurement model for estimating the air speed can be derived as

$$|\mathbf{v}_a| = \sqrt{\frac{2(p_{stag} - p_{stat})}{\rho_{air}}} = \sqrt{\frac{2p_{dyn}}{\rho_{air}}} \quad (5.21)$$

where ρ_{air} is the density of air.

5.4 Position Estimation Models

This section contains measurement models to estimate the position of the aircraft in the NED-frame. Since the altitude of the aircraft is handled explicitly in Section 5.2, the position is referred to as a two dimensional coordinate on the earth.

5.4.1 GPS

A measurement model to estimate the position of the aircraft in earth fixed coordinate system using the GPS can be derived as

$$\mathbf{x} = \mathbf{x}_{GPS} \quad (5.22)$$

where \mathbf{x}_{GPS} is the position indicated by the GPS.

5.5 Summarized Model

This section summarizes all equations that forms the Differential Algebraic Model (DAE) model of the UAV system. All variables denoted x_i and y_i are state variables and measurements respectively. Sensor faults denoted f_i are assumed to enter the system in the measurement equations. The total number of equations is 34 (16 measurement equations, 13 algebraic equations, and 5 differential equations).

5.5.1 Measurements Equations with Faults

In this section all measurement equations is presented. Bold variable represent vectors. The total number of measurement equations is 16.

$$\mathbf{x}_{mag} = \mathbf{y}_{mag} + \mathbf{f}_{mag} \quad (5.23)$$

$$\mathbf{x}_{acc} = \mathbf{y}_{acc} + \mathbf{f}_{acc} \quad (5.24)$$

$$\mathbf{x}_{gyro} = \mathbf{y}_{gyro} + \mathbf{f}_{gyro} \quad (5.25)$$

$$x_{stat} = y_{stat} + f_{stat} \quad (5.26)$$

$$x_{stat} = y_{stat} + f_{stat} \quad (5.27)$$

$$x_{GPS_c} = y_{GPS_c} + f_{GPS} \quad (5.28)$$

$$x_{vg} = y_{GPS_s} + f_{GPS} \quad (5.29)$$

$$x_{GPS_h} = y_{GPS_h} + f_{GPS} \quad (5.30)$$

$$x_{lat} = y_{GPS_{lat}} + f_{GPS} \quad (5.31)$$

$$x_{long} = y_{GPS_{long}} + f_{GPS} \quad (5.32)$$

5.5.2 System Equations

This section summarizes all differential and algebraic equations and inequalities in the DAE model of the UAV system. Bold variables represents vectors. The total number of system equations is 18 (13 algebraic equations, and 5 differential equations).

$$x_h = K \log \left(\frac{P_{s0}}{x_{stat}} \right) + h_0 \quad (5.33)$$

$$x_{va} = \sqrt{\frac{2(x_{stag} - x_{stat})}{\rho_{air}}} \quad (5.34)$$

$$x_{stag} \geq x_{stat} \quad (5.35)$$

$$x_{vg} = \sqrt{\dot{x}_{long}^2 + \dot{x}_{lat}^2} \quad (5.36)$$

$$\mathbf{x}_{mag} = R_b^n \mathbf{B} \quad (5.37)$$

$$|\mathbf{q}| = 1 \quad (5.38)$$

$$|\mathbf{x}_{mag}| = 1 \quad (5.39)$$

$$\mathbf{x}_{acc} = R_b^n \mathbf{g} + \mathbf{x}_{gyro} \times \begin{pmatrix} x_{va} \\ 0 \\ 0 \end{pmatrix} + \begin{pmatrix} a_i^b \\ 0 \\ 0 \end{pmatrix} \quad (5.40)$$

$$\dot{\mathbf{q}} = \frac{1}{2} S(\mathbf{x}_{gyro}) \mathbf{q} \quad (5.41)$$

$$x_{GPSc} = \tan^{-1} \left(\frac{2(q_1 q_2 + q_0 q_3)}{q_0^2 + q_1^2 - q_2^2 - q_3^2} \right) \quad (5.42)$$

$$|x_{va} - x_{vg}| \leq v_w \quad (5.43)$$

Part III

Results

6

Model Based Diagnosis System

The purpose of the Model Based Diagnosis System (MBDS) is to detect faults on a single autopilot. The MBDS consists of model based diagnosis techniques. On a multi autopilot system the MBDS can be used as a standalone diagnosis system on the individual autopilots, as a compliment to a hardware based diagnosis system. General approaches for designing a diagnosis system are presented in Chapter 2.

6.1 System Structure

The task of a diagnosis system is to generate a diagnosis statement S , which contains information about the behavior of the system. In order to structure the system, it is divided into smaller parts which is called diagnosis tests δ_i . Each diagnosis test generates a diagnosis statement S_i . The information in the statements S_i is combined to form the diagnosis statement S . The task of combining the statements S_i is handled by the decision logic, see Section 2.6. With this structure each statement S_i (generated by a diagnosis test δ_i), can be interpreted as a set of possible fault modes which the system might be in. Based on the information in the diagnosis statements S_i , the decision logic decides when to generate an alarm. Figure 6.1 shows the structure of the MBDS.

6.2 Workflow

The workflow in the task of designing diagnosis tests can be summarized as

1. Design a mathematical model of the UAV system (presented in Section 5).
2. Apply the MTES-algorithm (presented in Section 2.4.1) to the model to find

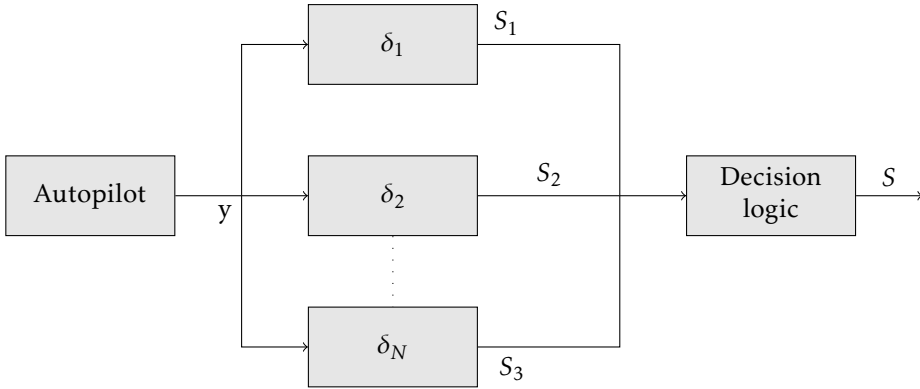


Figure 6.1: The structure of the model based diagnosis system.

the set of equations which can be used for test design. If the detectability and isolability performance is satisfactory go to **step 3**, otherwise rework the model in **step 1**.

3. If all test candidates on the MTES level are possible and manageable to implement, go to **step 6**. Elsewise implement the tests that is possible, then go to **step 4**.
4. Apply the TES algorithm (presented in Section 2.4.1) to find other test candidates. Investigate which test candidates that are sufficient to preserve the isolability in the system.
5. Implement the test candidates in step 4 that is possible and manageable to implement. If the isolability and detectability are preserved, go to **step 6**. Elsewise go back to **step 4**.
6. Evaluate the implemented tests in MATLAB using logged sensor data. If the result is satisfactory, go to **step 7**. Elsewise go back to **step 2**.
7. Implement the tests on the EasyPilot.

6.3 Results

In this section the final set of tests are presented together with an isolability analysis of the MBDS. The minimal set of fault modes presented in Section 2.3 is used through this section. The software implementation assumes that a single fault only enters the system in one equation. Due to this practical issue, the model of the UAV presented in Section 5.5 was augmented with four trivial equations according to:

$$x_{Fmag} = f_{mag} \quad (6.1)$$

$$x_{Facc} = f_{acc} \quad (6.2)$$

$$x_{Fgyro} = f_{gyro} \quad (6.3)$$

$$x_{FGPS} = f_{GPS} \quad (6.4)$$

where the faults f_{mag} , f_{acc} , f_{gyro} , and f_{GPS} are related to the dummy state variables x_{Fmag} , x_{Facc} , x_{Fgyro} , and x_{FGPS} , which in turn replaces the faults in the model. Thus, the faults only enters the system in one equation.

6.3.1 MTES Test Candidates

The test candidates obtained by applying the MTES-algorithm to the model of the UAV-system provides the decision structure according to Table 6.1. The set of six diagnosis tests provides the isolability according to Table 6.2.

Test	NF	F _{mag}	F _{GPS}	F _{gyro}	F _{acc}	F _{stag}	F _{stat}
$\delta_{2,1}$	0	X	0	0	0	0	0
$\delta_{2,2}$	0	0	X	0	0	0	0
$\delta_{2,3}$	0	0	0	X	0	0	0
$\delta_{2,4}$	0	0	0	0	X	0	0
$\delta_{2,5}$	0	0	0	0	0	X	0
$\delta_{2,6}$	0	0	0	0	0	0	X

Table 6.1: Decision structure of the test candidates, using the MTES-algorithm with minimal set of fault modes.

Fault	f_{mag}	f_{GPS}	f_{gyro}	f_{acc}	f_{stag}	f_{stat}
f_{mag}	X	0	0	0	0	0
f_{GPS}	0	X	0	0	0	0
f_{gyro}	0	0	X	0	0	0
f_{acc}	0	0	0	X	0	0
f_{stag}	0	0	0	0	X	0
f_{stat}	0	0	0	0	0	X

Table 6.2: Structural isolability matrix in the MBDS using the MTES-algorithm with minimal set of fault modes. Full structural isolability is obtained.

Each of the proposed MTESs consists of a set of 33 equations. The two test candidates $\delta_{2,1}$ and $\delta_{2,2}$ were possible to implement. The tests are implemented according to Section 6.3.4.

6.3.2 TES Test Candidates

The TES algorithm provides 63 TESs when applied on the model of the UAV-system. Since the test candidates given by the MTES algorithm is included in this set, only 57 new test candidates are obtained. The set of TESs provides full isolability, corresponding to the isolability matrix Table 6.2. Six test candidates with fault sensitivity according to Table 6.3 were possible to implement. The tests are implemented according to Section 6.3.4, and the isolability according to Table 6.4 is obtained by the TES test candidates.

Test	NF	F _{mag}	F _{GPS}	F _{gyro}	F _{acc}	F _{stag}	F _{stat}
$\delta_{3,1}$	0	X	0	X	0	0	0
$\delta_{3,2}$	0	X	0	0	X	0	0
$\delta_{3,3}$	0	0	X	0	0	0	X
$\delta_{3,4}$	0	0	X	0	0	X	X
$\delta_{3,5}$	0	0	0	0	0	X	X
$\delta_{3,6}$	0	X	0	X	X	0	0

Table 6.3: Decision structure of the implemented test candidates, using the TES-algorithm with minimal set of fault modes.

Fault	f_{mag}	f_{GPS}	f_{gyro}	f_{acc}	f_{stag}	f_{stat}
f_{mag}	X	0	0	0	0	0
f_{GPS}	0	X	0	0	0	X
f_{gyro}	X	0	X	0	0	0
f_{acc}	X	0	0	X	0	0
f_{stag}	0	0	0	0	X	X
f_{stat}	0	0	0	0	0	X

Table 6.4: Isolability matrix of the selected test candidates from the TES-algorithm, using the minimal set of fault modes. Faults in the magnetometer and static pressure sensor can be isolated. Faults in the gyroscopes and accelerometers can not be isolated from faults in the magnetometer. Faults in the GPS and stagnation pressure sensor can not be isolated from faults in the static pressure sensor.

6.3.3 Final Set of Tests

All tests in this section are implemented and evaluated in MATLAB using logged data from the UAV system. Plots of the residuals using logged data are presented for each of the tests presented in Section 6.3.4, together with a discussion of the outcome. The properties of an ideal residual are discussed in Section 2.2. More plots are available in Appendix A.2.

The set of final tests and the corresponding isolability are presented in Table 6.5. The associated decision structure is presented in Table 6.6. The last column in Ta-

ble 6.6 shows which of the tests that has been implemented on the EasyPilot during this work. Table 6.5 shows that faults in the magnetometer, GPS, and static pressure sensor are isolable. Faults in the gyroscope and accelerometer can't be isolated from faults in the magnetometer. Faults in the stagnation pressure sensor can not be isolated from faults in the static pressure sensor. It is desirable to be able to isolate faults in the gyroscope and accelerometer from faults in the magnetometer. This isolability can be obtained by designing a test which is sensitive to faults in the accelerometer and gyroscope only.

Fault	f_{mag}	f_{GPS}	f_{gyro}	f_{acc}	f_{stag}	f_{stat}
f_{mag}	X	0	0	0	0	0
f_{GPS}	0	X	0	0	0	0
f_{gyro}	X	0	X	0	0	0
f_{acc}	X	0	0	X	0	0
f_{stag}	0	0	0	0	X	X
f_{stat}	0	0	0	0	0	X

Table 6.5: Isolability matrix in the model based diagnosis system.

Test	NF	F_{mag}	F_{GPS}	F_{gyro}	F_{acc}	F_{stag}	F_{stat}	EasyPilot
$\delta_{2,1}$	0	X	0	0	0	0	0	Yes
$\delta_{2,2}$	0	0	X	0	0	0	0	No
$\delta_{3,1}$	0	X	0	X	0	0	0	No
$\delta_{3,2}$	0	X	0	0	X	0	0	Yes
$\delta_{3,3}$	0	0	X	0	0	0	X	Yes
$\delta_{3,4}$	0	0	X	0	0	X	X	Yes
$\delta_{3,5}$	0	0	0	0	0	X	X	No
$\delta_{3,6}$	0	X	0	X	X	0	0	Yes

Table 6.6: Decision structure in the model based diagnosis system. With no zero column the in the decision structure all faults are detectable. The column **EasyPilot** tells which tests that has been implemented on the EasyPilot.

6.3.4 Residual generation

This section describes how the residuals of the final set of tests presented in Section 6.3.3 are generated.

Test $\delta_{2,1}$

The fault signature of test $\delta_{2,1}$ is presented in Table 6.6. Since the length of the field vector of the earth's magnetic field is constant in the NED-frame, the length should be constant in the body-frame as well. This means that the length of measured magnetic field vector should be constant. However, since the magnetometer is calibrated on a unit sphere the calibrated measurements from the

magnetometer should have length one if the magnetometer is working properly. Hence, a residual can be generated as

$$r_{2,1} = |\mathbf{x}_{mag}| - 1 \quad (6.5)$$

Where \mathbf{x}_{mag} are the calibrated measurements from the magnetometer. Test $\delta_{2,1}$ is evaluated using a logged dataset. The autopilot is mounted on the airframe, with the engine running at 100% of maximum power at time $t \in [4, 5]$ and 50% of maximum power at time $t \in [10, 15]$. In order to enhance the effect of disturbances, shielded cable where not used during the evaluation. Magnetic items and electric wires in the environment on the airframe introduces perturbations which corresponds to both soft iron perturbations and hard iron perturbations. Theoretically the effect of constant magnetic perturbations can be reduced by proper calibration, i.e., to use a dataset with the autopilot mounted on the airframe for calibration. In practice this is an issue since the calibration dataset must excite all modes in the magnetometer, which means that the whole airframe must be twisted and turned, be put upside down, etc. Due to this issue the calibration is not performed with the autopilot mounted on the airframe. The calibration algorithm is described in Section 4.3.2. A plot of the residual and the CUSUM test quantity is presented in Figure 6.2

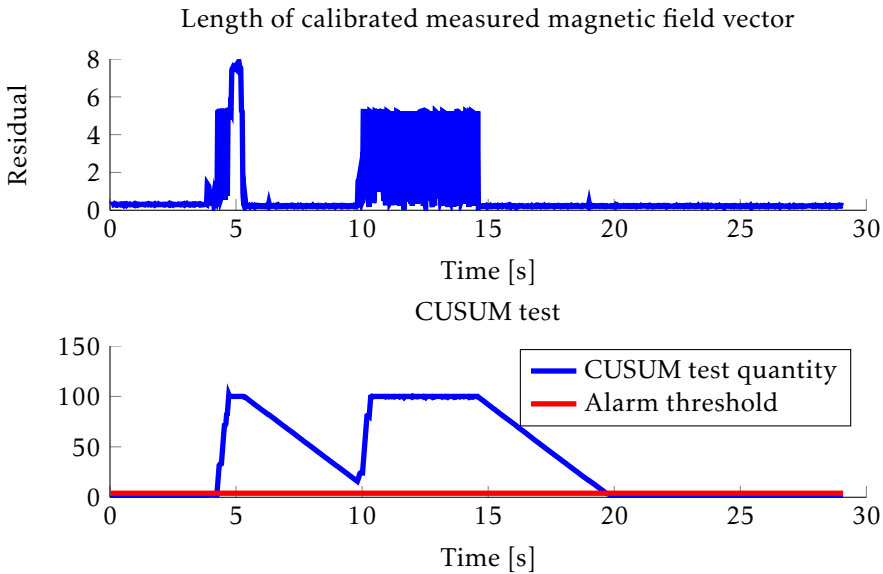


Figure 6.2: Test $\delta_{2,1}$, residuals and CUSUM test quantity. The CUSUM test quantity is upper limited to 100.

The small bias in the residuals is due to magnetic perturbations on the airframe, that are not taken into account during the calibration. However, the injected

faults at time $t \in [4, 5]$ and $t \in [10, 15]$, are clearly noticeable in the residual and the CUSUM test generates an alarm almost immediately when the fault is introduced in the system. Thus, the residual is sensitive to the faults that it was intended for.

Test $\delta_{2,2}$

The fault signature of test $\delta_{2,2}$ is presented in Table 6.6. The GPS indicates both speed and position, as described in Section 4.5. The speed of the aircraft can be estimated from the position according to (5.36). Hence a residual can be generated as

$$\tilde{r}_{2,2} = x_{vg} - \sqrt{\dot{x}_{long}^2 + \dot{x}_{lat}^2} \quad (6.6)$$

Where x_{vg} is the ground speed and x_{long} , x_{lat} is the position in longitude and latitude. The position must be converted to a distance in SI-units to work properly with the speed indication. By modeling the Earth as a sphere, the distance on the sphere between two points is given as

$$d = r\Delta\hat{\sigma}(x_{long}, x_{lat}) \quad (6.7)$$

where r is the radius of the Earth and $\Delta\hat{\sigma}$ is the central angle between the points on the sphere. The central angle $\Delta\hat{\sigma}$ is given by Vincenty's formula, presented in Section A.1. Using Vincenty's formula, the residual can be expressed as

$$r_{2,2} = x_{vg} - \frac{d}{dt}(r\Delta\hat{\sigma}(x_{long}, x_{lat})) \quad (6.8)$$

The residual and CUSUM test quantity are presented in Figure 6.3. At time $t = 80$ the dataset is manipulated with a variance fault with a magnitude of 5 m, in the position measurements. The fault is detected, and the CUSUM test generated as alarm. The estimate of the speed given by the position is given by the difference between the momentary position and the last known position, thus the residual will not be sensitive to constant bias faults in the position indicated by the GPS. Hence, the residual is sensitive to variance faults in the position estimate but not to bias faults. Thus, the residual is sensitive to some of the fault that it is intended for, but for example bias faults will cause missed detections.

Test $\delta_{3,1}$

The fault signature of test $\delta_{3,1}$ is presented in Table 6.6. The attitude of the aircraft can be estimated from both the magnetometer and the gyroscopes according to Section 5.1. An estimate of the attitude based on Equation 5.13 will suffer from integration drift of the gyroscope and hence the estimate will be poor. To work around this problem the measurements from the gyroscopes can be combined with the measurements from the magnetometer. The attitude of the aircraft can

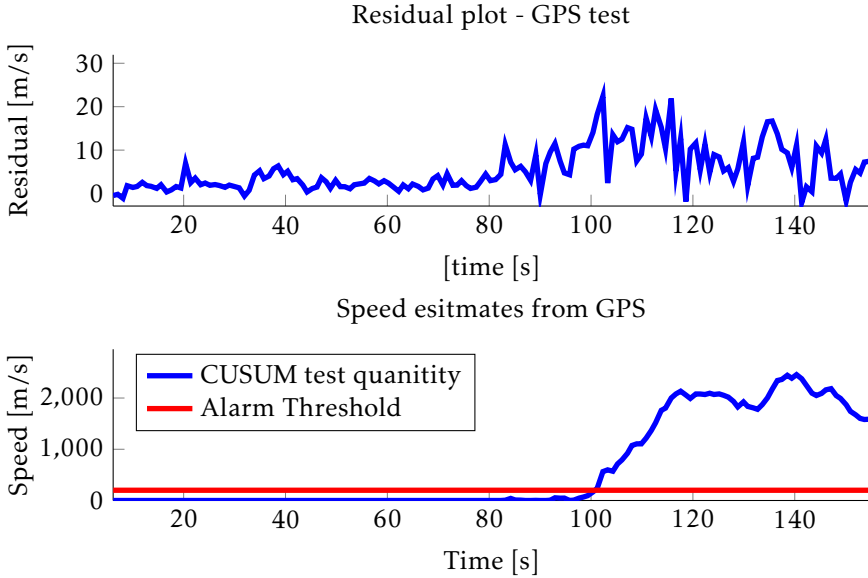


Figure 6.3: Test $\delta_{2,2}$ residual. The residual have a bias of circa 2 m/s, but the occurrence of a fault at time $t = 80$ is easy to distinguish from the fault free case.

be predicted by discretization of Equation (5.41), using an Euler forward approximation

$$\mathbf{q}_{k+1} = \frac{T_s}{2}(S(\mathbf{x}_{gyro}) + \mathbf{I})\mathbf{q}_k \quad (6.9)$$

Where T_s is the sample time. Prediction over an arbitrary horizon ξ is obtained by substitute \mathbf{q}_k with \mathbf{q}_{k+1} repeatedly and hence get an estimate of $\mathbf{q}_{k+\xi}$. The quaternion \mathbf{q} represents the attitude estimate of the aircraft. The attitude can be estimated by the magnetometer by estimating the rotation matrix R_b^n between body-frame and NED-frame. The task of estimating all elements in the 3 by 3 rotation matrix is not trivial, due to the constraint that the rotation matrix must be special orthogonal, i.e., its determinant must equal one. For good results the estimation requires some filtering. To get a good estimate of the rotation matrix an EKF can be to keep track of the quaternions that defines the rotation matrix, as described in Magnusson [2013] and Veiback [2010]. The disadvantage of using such a large filter is that measurements from the GPS, gyroscopes, magnetometers, and accelerometers are used to estimate the rotation matrix, and the test will be sensitive to fault in these sensors as well. For this application an EKF that only uses the magnetometers as measurement update should also be considered instead. The estimate from this filter will not be as accurate as the estimate from a more complex filter, but the test will remain sensitive to faults in the magne-

tometer and gyroscopes only. The smaller filter can also be used as backup filter on the UAV system, which will be further discussed in Section 8.2. Residuals are generated as the difference between the predicted attitude from the gyroscopes and the estimate from the EKF, see (6.10).

$$r_{3,1} = \mathbf{q}_{k+\xi} - \mathbf{q}_{EKF} \quad (6.10)$$

A plot of the residuals are presented in Figure 6.4. The residuals is unbiased and seems to alternate around zero. At time $t = 60$ a bias fault of the same magnitude as the gyro bias in Table 4.1 is introduced. As seen in the figure, the introduced fault increases the variance of the residuals. Thus, the variance of the residual could be used as a distance measure in the CUSUM test.

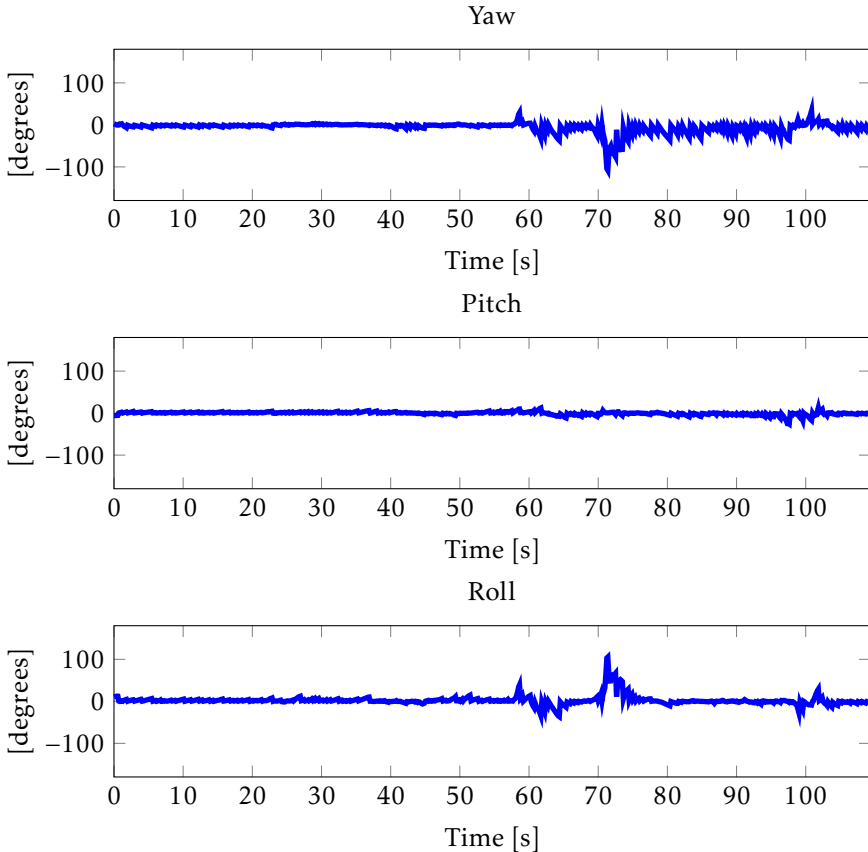


Figure 6.4: Test $\delta_{3,1}$, residual and CUSUM test quantity. During this test the gyro prediction horizon is approximately half a second.

Test $\delta_{3,2}$

The fault signature of test $\delta_{3,2}$ is presented in Table 6.6. The NED-frame and the body-frame is related by a rotation matrix, which by definition is an orthogonal matrix. As a linear transformation an orthogonal matrix preserves dot products, hence the dot product between the gravity vector and the magnetic field vector should be equal in the NED-frame and the body-frame. A residual can be generated as

$$r_{3,2} = \mathbf{y}_{acc}^b \cdot \mathbf{y}_{mag}^b - \mathbf{g}^N \cdot \mathbf{B}^N \quad (6.11)$$

Where \mathbf{y}_{acc}^b and \mathbf{y}_{mag}^b is the measurements from the accelerometer and magnetometer in the body-frame, and \mathbf{g}^N and \mathbf{B}^N is the magnetic field vector and gravity vector in the NED-frame. If the accelerometers measurements is compensated for centripetal acceleration and the acceleration caused by thrust according to (5.40), the test will be sensitive to faults in the gyroscopes and the pressure sensors as well. If the measurements is not compensated for external acceleration, the measurement model will contain higher uncertainty.

In order to evaluate the test, a dataset with the autopilot mounted on the airframe was collected. Figure 6.5 shows the residual and the CUSUM test quantity while the engine of the aircraft is running. The engine generates a magnetic field that interferes with the magnetic field of the earth. The perturbations corresponds to hard iron errors. Magnetic errors is thoroughly described in Renaudin et al. [2010]. At time $t \in [4, 5]$ the engine is raised from zero to maximum power. At time $t \in [10, 15]$ the engine is raised from zero to 50% of maximum power. With the engine running at 100% the measured magnetic field is in magnitude around seven times the earth's magnetic field.

The small bias in the residuals is due to magnetic perturbations on the airframe, that are not taken into account during the calibration. The fault that occurs when the magnetometer is disturbed by the engine, is easy to distinguished in the residual and the CUSUM test quantity generates an alarm. The only disadvantage with the test is that heavy accelerations may give rise to false alarms, since external accelerations will occur as faults in this test. One way to solve this issue is to deactivate the test when the aircraft is in take off, landing, or loiter mode.

Test $\delta_{3,3}$

The fault signature of test $\delta_{3,3}$ is presented in Table 6.6. The height over sea level can be estimated separately from the static pressure and the GPS. Since the autopilot is not equipped with a temperature sensor, the gain K is approximated by assuming a constant temperature. A residual can be generated as

$$r_{3,3} = x_{GPS_h} - K \log\left(\frac{P_{s0}}{x_{stat}}\right) - h_0 \quad (6.12)$$

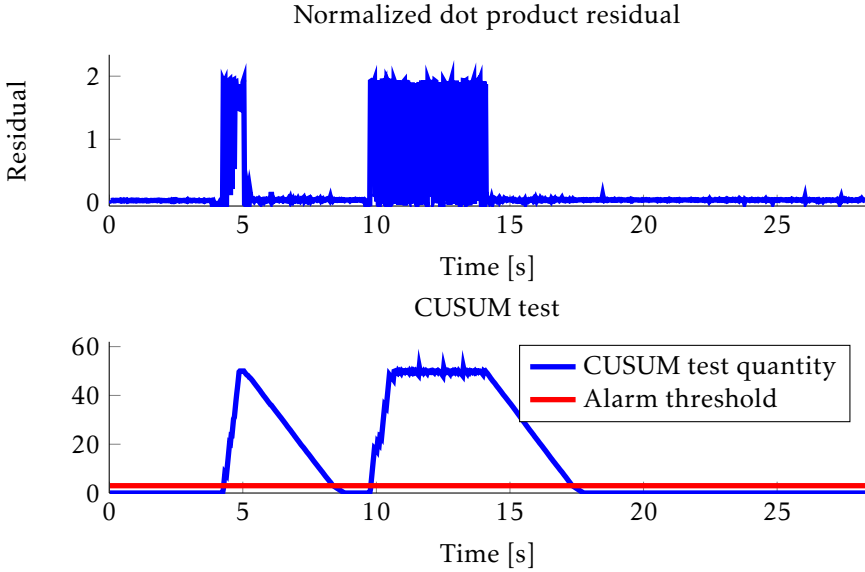


Figure 6.5: Test $\delta_{3,2}$, residual and CUSUM test quantity. At time $t \in [4, 5]$ and $t \in [10, 15]$ magnetic faults are introduced in the system, which are clearly visible in the figure.

Where x_{GPS_h} is the indicated height by the GPS, K is determined by (5.17), P_{s0} is the pressure at ground level, and x_{stat} is the measure static pressure. To evaluate the test in a proper way a dataset with the presence of a fault in the GPS during a real flight is used.

Figure 6.6 shows the residual and the CUSUM test quantity. The residual is unbiased and alternates around zero when no fault is present. A fault in the GPS occurs at time $t = 150$ and is clearly noticeable in the residual, which can be seen in the figure. A fault of the same magnitude in the static pressure sensor, would have forced the residual to go to a corresponding positive value. Thus, the residual have sufficient properties to be useful in practice.

Test $\delta_{3,4}$

The fault signature of test $\delta_{3,4}$ is presented in Table 6.6. The ground speed is indicated by the GPS and the air speed can be estimated from the pressure sensors, according to Section 5.3. A residual can be generated as

$$\tilde{r}_{3,4} = |\mathbf{x}_{vg}| - |\mathbf{x}_{va} + \mathbf{v}_w| \quad (6.13)$$

Where \mathbf{x}_{vg} is the ground speed, \mathbf{x}_{va} is the air speed, and \mathbf{v}_w is the wind speed. This model requires an estimate of the wind speed, since there is no sensor to measure the wind speed on the autopilot. In Magnusson [2013] a method for estimating

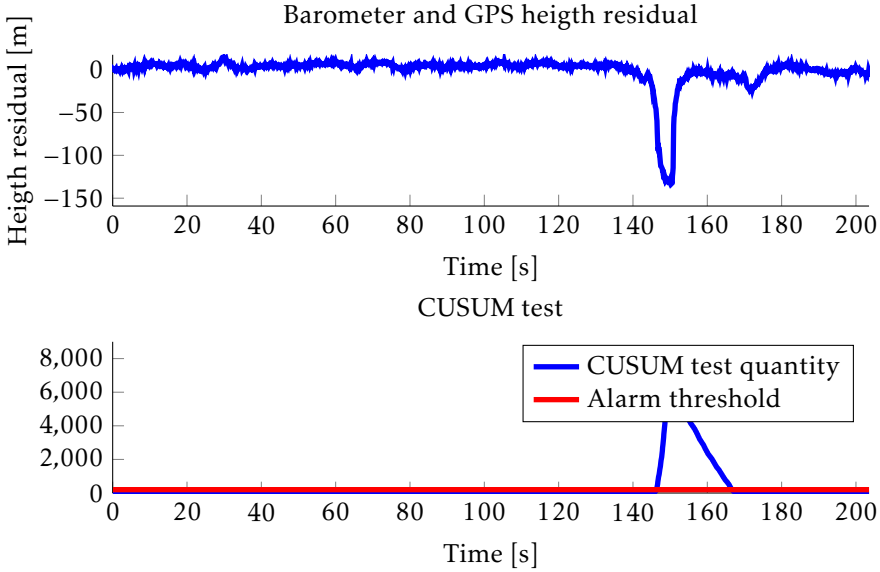


Figure 6.6: Test $\delta_{3,3}$, residual and CUSUM test quantity. A fault in the GPS is introduced at time $t \in [145, 155]$, which is easy to distinguish in the residual.

the wind speed using a EKF is presented. The disadvantage with such a complex filter is that the estimate of the wind speed becomes correlated to all the sensors measurements that are used to update the filter, which means that the test will be sensitive to faults in other sensors as well. A more rough approximation is to assume that the wind speed is zero and use a higher threshold on the residuals. The threshold corresponds to the maximum allowable wind speed that the UAV. By using this approach the test will generate an alarm if the wind speed is to high as well, which could be useful for the operator. A residual can be generated as

$$r_{3,4} = |\mathbf{x}_{vg}| - |\mathbf{x}_{va}| \quad (6.14)$$

Figure 6.7 shows the residuals and the CUSUM test quantity using a dataset from a real flight. As seen in the figure, the residual have a bias which could be interpreted as the aircraft is moving along with the wind most of the time, or that a small bias fault is present in one of the sensors. At time $t = 140$ the residual reaches 23 m/s and the CUSUM tests generates an alarm. Since there is no estimate of the wind speed available, the alarm could be interpreted as strong winds or a fault in any of the sensors. Thus, the residual is sensitive to faults in both the pressure sensors and faults in the GPS measurements. The residual is however also sensitive to strong winds, i.e., strong winds could generate false alarms. False alarms are not desirable, but in this application false alarms are related to strong winds, which the operator could see as a warning.

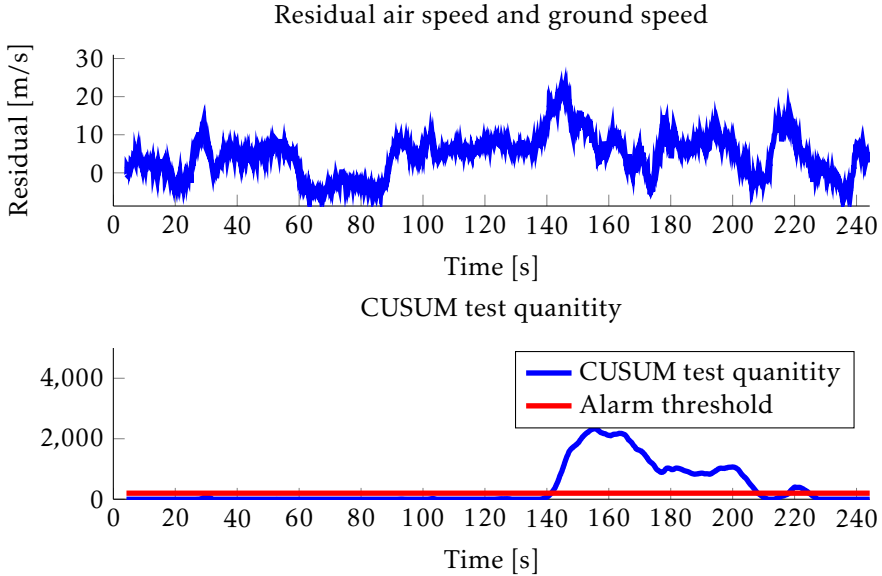


Figure 6.7: Test $\delta_{3,4}$, residual and CUSUM test quantity during a flight. At time $t = 140$ the test generates an alarm.

Test $\delta_{3,5}$

The fault signature of test $\delta_{3,5}$ is presented in Table 6.6. When the aircraft is moving, the stagnation pressure should always be greater than the static pressure. A non-linear residual can be generated as

$$r_{3,5} = \max(0, x_{stat} - x_{stag}) \quad (6.15)$$

Where x_{stat} is the measured static pressure and x_{stag} is the measured stagnation pressure. A non-zero output from the residual generator corresponds to higher static pressure than stagnation pressure. For properly working sensors this should not be possible. Due to measurement noise in the sensors the static pressure could exceed the stagnation pressure when the aircraft is moving slowly. A way to get rid of this problem is to only consider the result of the test when the speed indicated by the GPS is higher than a certain level. Another way to reduce the effect from measurement noise is to apply the CUSUM test.

A dataset from a real flight is used to evaluate the test. Plots of the residual and CUSUM test quantity are presented in Figure 6.8. In the fault free scenario the residual equals zero. When a fault occurs at time $t = 320$ the residual goes to a non-zero value, which is easy to distinguish in the figure. The fault corresponds to a higher stagnation pressure than static pressure, i.e., a negative dynamic pressure. Since the residual is defined as an inequality, it is not sensitive to a drop in the

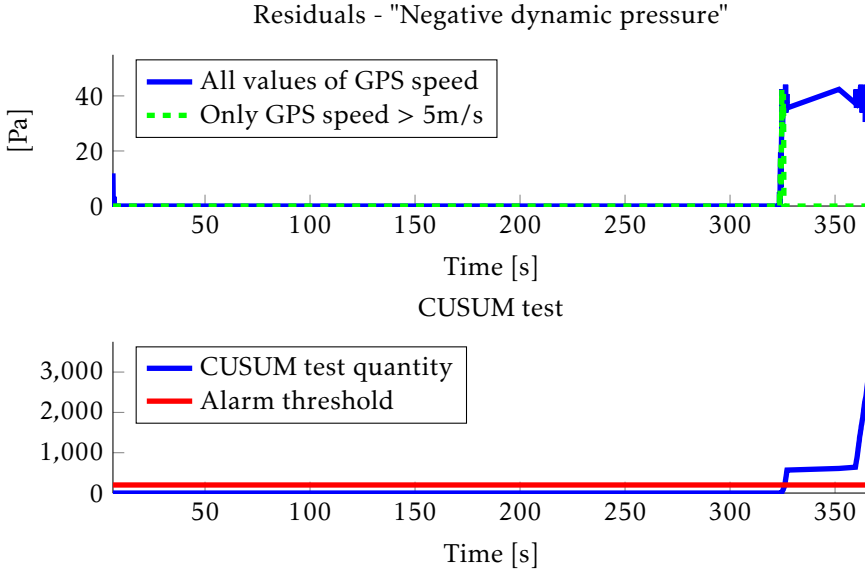


Figure 6.8: Test $\delta_{3,5}$, residuals and CUSUM test quantity during a flight.

static pressure sensor, or vice versa, a peak in the stagnation pressure sensor. However, in a real application the most common fault in the stagnation pressure sensor is when a small particle get stuck in the pitot tube which is attached to the sensor, causing a pressure reduction which is visible in the residual.

Test $\delta_{3,6}$

The fault signature of test $\delta_{3,6}$ is presented in Table 6.6. On the EasyPilot the explicit complementary filter described in Veiback [2010] is used to estimate the rotation matrix during flights, using measurements from the gyroscopes, magnetometers, and accelerometers. With a good estimate of the rotation matrix several tests can be performed, although all such test will be sensitive to fault in all sensors used to estimate the rotation matrix in the explicit complementary filter. Hence all tests based on the explicit complementary filter are at least sensitive to faults in the gyroscopes, magnetometers, and accelerometers.

By rotating the reference magnetic field vector in the NED-frame into the body-frame a residual can be generated as

$$\mathbf{r}_{3,6} = \mathbf{x}_{mag} - R_b^N \mathbf{B} \quad (6.16)$$

Where \mathbf{x}_{mag} is the calibrated measurement from the magnetometer and \mathbf{B} is the normalized magnetic field vector in the NED-frame. To evaluate this test a dataset was collected while the autopilot was rotated around its axes. To get a scalar residual a residual generator can be expressed as

$$\tilde{r}_{3,6} = |\mathbf{r}_{3,6}| \quad (6.17)$$

Figure 6.9 shows the residuals and the CUSUM test quantity during a flight when no fault occurs. The residuals are unbiased and alternates around zero. Since attitude of the aircraft is obtained from the log data, it is not possible to inject a fault in the gyroscope or accelerometer to analyze how the fault propagates to the residuals. However, the properties of the residuals in the fault free case is satisfying, but the propagation of faults in the gyroscope and accelerometer to the residual must be further evaluated. To order evaluate the test further a model of the attitude estimation filter is needed.

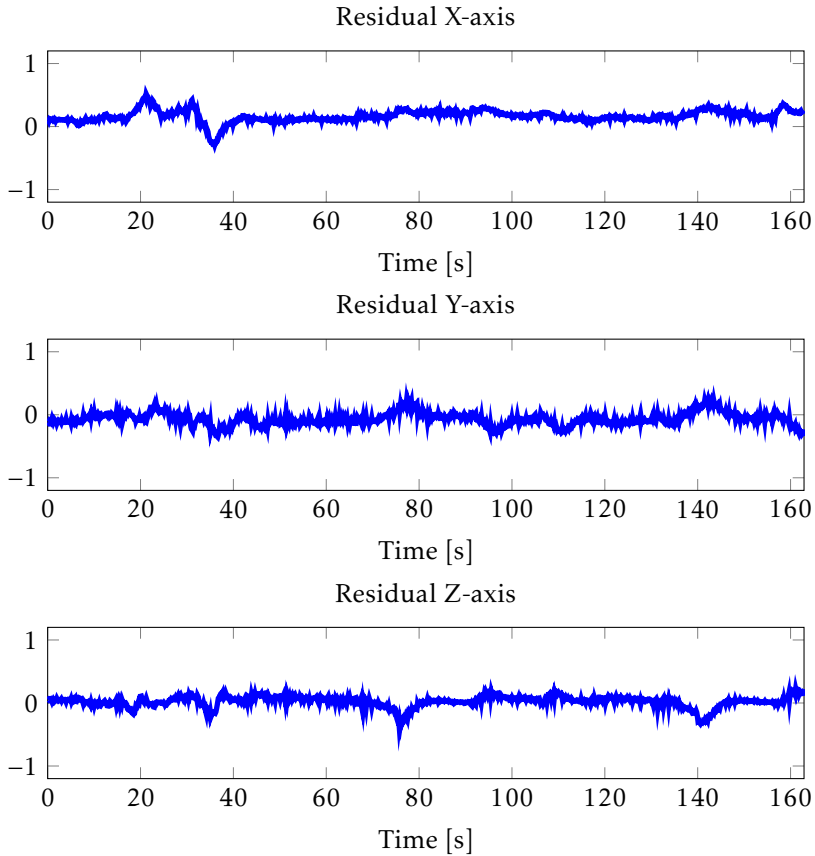


Figure 6.9: Test $\delta_{3,6}$ residuals in the fault free case.

7

Triple Redundant Autopilot

One possible way to increase the reliability of the UAV is to use several autopilots on a single airframe. The use of several autopilots introduces hardware redundancy in the system, which can be used for hardware diagnosis as described in Section 2.

The Triple Redundant Autopilot (TRA) consists of three individual autopilots on a single airframe. In this chapter the design process of a TRA is analyzed. In the design process there are several general choices and aspects that need to be analyzed, depending on the available hardware and the application. The proposed design is based on a system containing three identical EasyPilots, intended to be used for small UAVs.

7.1 Components

In this section the necessary components in the system is presented. In certain applications the system must be able to communicate with additional components or payloads. Since the integration of external components or payloads are very system specific, it will not be in the scope of this thesis.

7.1.1 Autopilot

Each autopilot is assumed to be equipped with a set of sensors and an Attitude Heading Reference System (AHRS) to estimate the states of the aircraft. An additional assumption is that the autopilots are equipped with a control system, to be able to control the aircraft. If the autopilots are equipped with an diagnosis system, there might be of interest to integrate this system with the TRA.

7.1.2 Supervisor Unit

The Supervisor Unit (SU) is the most central component in a TRA. Hardware diagnosis is performed in the SU and hence also the decision of which autopilot who is in best condition to control the aircraft. Since there exist only one SU, it is the most vital component in the system. To minimize the risk of an internal error or fault in the SU, as much functionality as possible should be placed in the autopilots.

7.1.3 Modem

The modem is used for communication between the ground station and the UAV. The UAV receives references for the controllers and transmits its current states to the operator on the ground.

7.1.4 Servo

The servo receives control signals from the TRA and sets the rudder and throttle on the UAV.

7.2 Communication

The information that needs to be exchanged by the components in the system is presented in this section. Since the EasyPilot is equipped with Controller Area Network (CAN), this is used as communication bus between the autopilots and the supervisor.

7.2.1 Sensor Data and Estimated States

To be able to perform hardware diagnosis by comparing sensor data or estimated states from the individual autopilots, sensor data and estimated states must be transmitted from the autopilots to the SU.

7.2.2 Control Signals and Servo

To be able to perform hardware diagnosis by comparing control signals between the individual autopilots, control signals must be transmitted from the autopilots to the SU. The control signals to the servos can either be transmitted by the SU or by the autopilots by introducing a mux which is controlled by the SU, as shown in Figure 7.1 and 7.2. The advantage with the mux approach is that the servo will always receive a control signal, even if the SU stops working. In order to prevent windup and enable soft transitions between the autopilots, the control signal that is transmitted to the servos must be transmitted to the autopilots as well. The autopilots themselves don't know if they are in control or not, hence the integral terms in the autopilots that isn't in control must be compensated with true control signals.

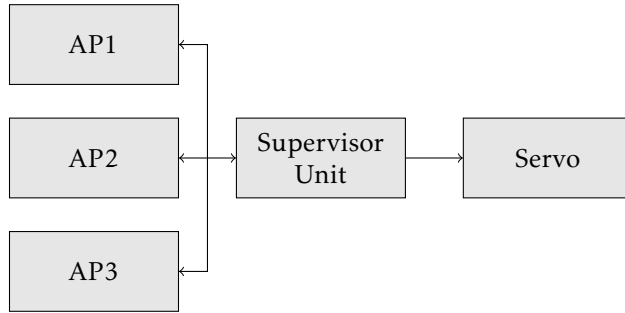


Figure 7.1: Servo communication setup 1: Communication between servo and SU.

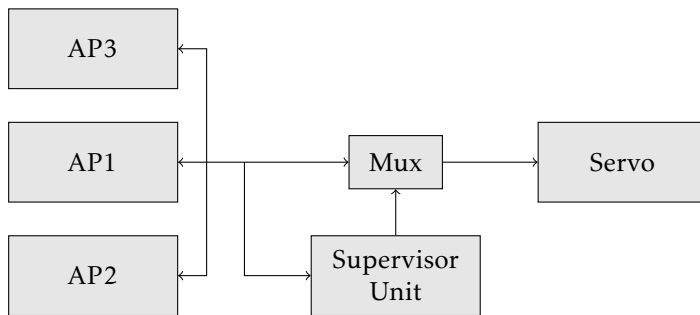


Figure 7.2: Servo communication setup 2: Communication between autopilots and servo using a mux controlled by the supervisor.

7.2.3 Diagnosis Data

If the autopilots is equipped with a diagnosis system, for example the system presented in Section 6, it is desirable to integrate this system to work in symbiosis with the hardware redundancy. Hence diagnosis data from the individual autopilots should be transmitted to the supervisor to be weighted in to the decision logic.

7.2.4 Modem Communication

The system could contain one or several modems. The use of several modems increases the reliability in the system since faults might be present in the modem as well as in any other component. On the airframe used in this thesis only one modem at the time can use the antenna. A second modem could be used as backup modem. The backup modem could be connected to the supervisor unit together with the first modem using a switch, or it could be connected to any of the autopilots. The setups are presented in Figure 7.3 and 7.4.

Which setup to use depends on the reliability to the SU, the modems, and the performance of the TRA compared to a single autopilot. Setup 1 will keep the

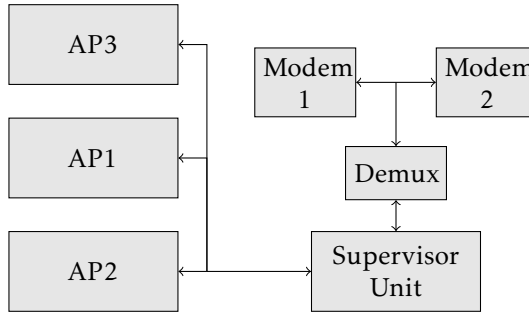


Figure 7.3: Modem communication setup 1: A modem and a backup modem connected to the supervisor using a switch. In case of a fault in the modem, the backup modem is used for communication with the ground control station instead.

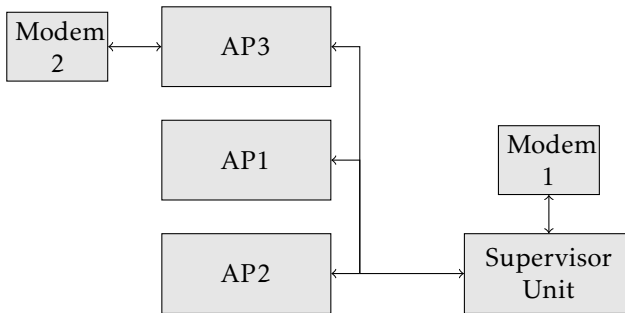


Figure 7.4: Modem communication setup 2: The backup modem is connected to an arbitrary autopilot. In case of a fault in the modem or the supervisor unit, the autopilot connected to the backup modem will control the aircraft.

triple redundant functionality even if the a modem is lost, but it is however more vulnerable to a fault in the SU.

7.2.5 Synchronization

One way to achieve synchronized communication on the CAN bus is to let the supervisor ask for information from the autopilots in a predetermined frequency. Using this method the autopilot can run their control algorithms asynchronous from each other, as long as they only update the integral term in the controller first when the supervisor unit ask for information.

7.2.6 Controller Area Network

Controller Area Network is the communication channel between the autopilots and the supervisor. CAN is a multi-master broadcast serial bus which is primarily intended for vehicles. CAN allows multiple control units to send messages

to each other in a safe and quick way. Technical details can be found in Texas-Instruments [2008]. The supervisor and the autopilots are connected on the CAN bus. The messages on the CAN-bus is presented in Table 7.1. To enable communication with the ground control station, i.e., uploading waypoints, routes, and control parameters the proposed CAN-protocol must be extended.

Message	Identifier	Data	Source	Destination
Attitude1	101,201,301	Yaw, Pitch	AP1,2,3	SU
Attitude2	102,202,302	Roll, GPS course	AP1,2,3	SU
GPS1	103,203,303	Longitude, Latitude	AP1,2,3	SU
GPS2	104,204,304	Ground speed, Altitude	AP1,2,3	SU
Analog	105,205,305	Air speed, Altitude	AP1,2,3	SU
Servo1	110,210,310	Ailerons, Elevator	AP1,2,3	SU
Servo2	111,211,311	Rudder, Throttle	AP1,2,3	SU
Servo3	112,212,312	Nosewheel	AP1,2,3	SU
Control1	1000	Ailerons, Elevator	SU	AP1,2,3
Control2	1001	Rudder, Throttle	SU	AP1,2,3
Control3	1002	Nosewheel	SU	AP1,2,3

Table 7.1: Message protocol for communication between the autopilots and the supervisor on the CAN-bus.

7.3 Hardware Diagnosis

Measurements from the sensors, estimated states, and control signals from each autopilot can be used to detect faults in the individual autopilots. In this section a set of fault modes are proposed and a set of diagnosis tests are presented.

7.3.1 Fault Modes

The concept of fault modes is described in Section 2.3. The notation F_{mode}^n will be used to represent a fault mode in autopilot n . As an example F_{gyro}^2 represents a fault in the gyroscopes in autopilot 2.

Sensor faults

The set of fault modes used in the MBDS could be used in the TRA as well, see Table 7.2. This set is used to detect and isolate sensor faults.

State faults

An alternative set of fault modes can be obtained by analyzing the estimated states in each autopilot instead of the raw sensor measurements. Since the measurements from the sensors are used to update the filter, faults in the sensor will appear as faults in the estimated states as well. If the filter is not working properly, i.e., the state estimation will be poor even in the case when no sensor fault is present. The state fault modes are presented in Table 7.3.

Fault mode	Description
F_{mag}	Fault in the magnetometer.
F_{acc}	Fault in the accelerometer.
F_{gyro}	Fault in the gyroscope.
F_{GPS}	Fault in the GPS.
F_{stag}	Fault in the stagnation pressure sensor.
F_{stat}	Fault in the static pressure sensor.

Table 7.2: Fault modes corresponding to sensor faults.

Fault mode	Description
F_{att}	Fault in the attitude estimate.
F_{pos}	Fault in the position estimate.
F_{vel}	Fault in the velocity estimate.
F_{alt}	Fault in the altitude estimate.

Table 7.3: Fault modes corresponding to state faults.

Actuator faults

A fault mode is defined for each actuator on the aircraft, according to Table 7.4.

Fault mode	Description
F_{ail}	Fault in the aileron control signal.
F_{ele}	Fault in the elevator control signal.
F_{rud}	Fault in the rudder control signal.
F_{thr}	Fault in the throttle control signal.
F_{nv}	Fault in the nose wheel control signal.

Table 7.4: Fault modes corresponding to actuator faults.

7.3.2 Diagnosis Tests

The concept of diagnosis tests are presented in Section 2.4. The diagnosis sub-statements generated from the diagnosis test will be denoted $S_{mode}^{n,m}$. As an example $S_{gyro}^{1,2}$ is the sub-statement corresponding to sensor test using the residual generator in Equation (7.1).

Sensor Tests

Using three autopilot with the same set of sensors, residuals can be generated as

$$r_k^{1,1} = y_k^1 - y_k^2 \quad (7.1)$$

$$r_k^{1,3} = y_k^1 - y_k^3 \quad (7.2)$$

$$r_k^{2,3} = y_k^2 - y_k^3 \quad (7.3)$$

where y_k^1, y_k^2, y_k^3 are measurements of the quantity k from identical sensors in the autopilots. The pairwise differences between measurements from identical sensors should be close to zero if no fault is present in the system.

State Tests

Using three autopilot with the same set of sensors and identical filters for state estimation, residuals can be generated as

$$r_k^{1,1} = \hat{x}_k^1 - \hat{x}_k^2 \quad (7.4)$$

$$r_k^{1,3} = \hat{x}_k^1 - \hat{x}_k^3 \quad (7.5)$$

$$r_k^{2,3} = \hat{x}_k^2 - \hat{x}_k^3 \quad (7.6)$$

where $\hat{x}_k^1, \hat{x}_k^2, \hat{x}_k^3$ are estimates of the state k in the autopilots. The pairwise differences between state estimates should be close to zero if no fault is present in the system.

Actuator Tests

Using three autopilot with the same set of sensors, identical filters for state estimation, and identical controllers residuals can be generated as

$$r_k^{1,2} = u_k^1 - u_k^2 \quad (7.7)$$

$$r_k^{1,3} = u_k^1 - u_k^3 \quad (7.8)$$

$$r_k^{2,3} = u_k^2 - u_k^3 \quad (7.9)$$

where u_k^1, u_k^2, u_k^3 is the control signals to the servo k , from the autopilots. The pairwise differences between the control signals should be close to zero if no fault is present in the system.

Test Selection

By choosing different sets of test depending on the current system mode, the total number of active tests can be reduced without affecting the diagnosability performance. In this system, it is sufficient to only perform state tests and actuator tests while the system is in the fault free mode. The sensor tests are active only when a state fault already is detected, in order to isolate the fault to a specific sensor.

The set of sensor faults that is activated depends on what kind of state fault that is detected, see Table 7.5.

State fault mode	Possible fault
F_{att}	$f_{mag}, f_{acc}, f_{gyro}$.
F_{pos}	f_{GPS} .
F_{vel}	$f_{GPS}, f_{stat}, f_{stag}$.
F_{alt}	f_{GPS}, f_{stat} .

Table 7.5: State fault modes and possible sensor faults.

7.3.3 Voting

The method of comparing the pairwise differences of N identical units is called voting. Voting algorithms are used to improve the reliability in N-Modular Redundant hardware systems. The concept of voting and several algorithms are presented in Latif-Shabgahi et al. [2004]. The decision structure for voting using three identical units can be generalized according to Table 7.6. This general approach is valid for all diagnosis tests presented in Section 7.3.2 and provides full isolability for all fault modes.

Test	Autopilot 1	Autopilot 2	Autopilot 3
$\delta_{mode}^{1,2}$	X	X	0
$\delta_{mode}^{1,3}$	X	0	X
$\delta_{mode}^{2,3}$	0	X	X

Table 7.6: The decision structure for voting using three autopilots.

As an illustration consider the sensor measurements in Figure 7.5, where the a fault is present in sensor 3. The corresponding residuals generated by 7.1 - 7.3, are presented in Figure 7.6. The fault is detected by the CUSUM algorithm which generates the alarms $\delta_i^{1,3}$ and $\delta_i^{2,3}$ when the test quantities exceeds the thresholds, see Figure 7.7. The fault is isolated to autopilot 3 by Table 7.6.

7.3.4 Detectability and Isolability

All sensor faults and actuator faults are detectable and isolable in the TRA.

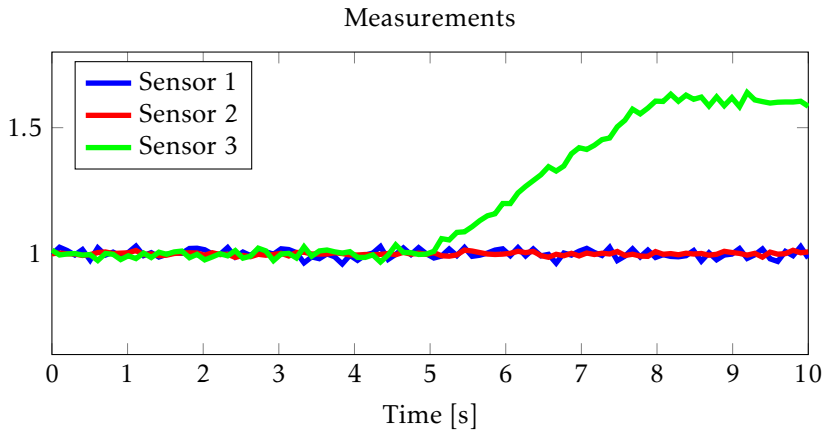


Figure 7.5: Three sensors measuring the same quantity. After 5 seconds a fault is present in sensor 3.

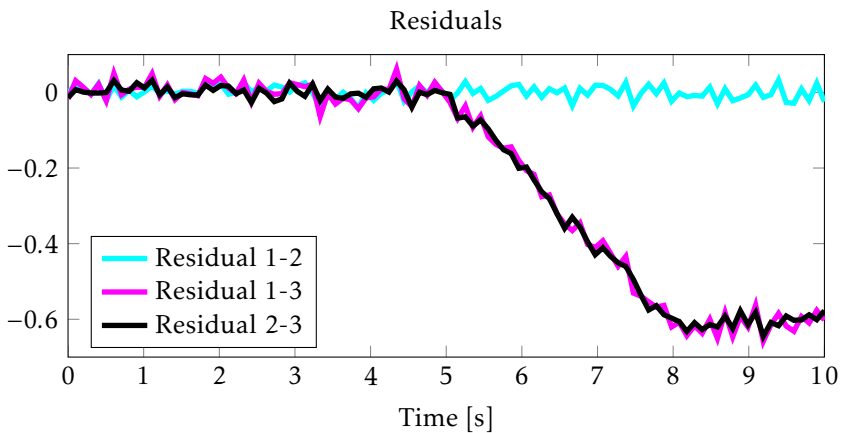


Figure 7.6: Residuals corresponding to Figure 7.5.

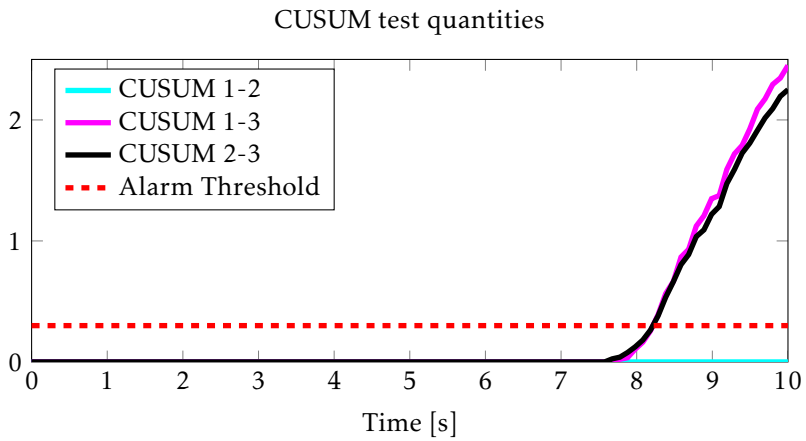


Figure 7.7: CUSUM test quantities corresponding to Figure 7.5.

8

Conclusions and Future Work

8.1 Conclusions

The primary goal with the master thesis was to design a system for detecting sensor faults on an autopilot system. The second objective is to evaluate how three autopilots on a single airframe could be used to increase the reliability of the aircraft. The model based diagnosis system is discussed in Section 8.1.1 and the triple redundant autopilot is discussed in Section 8.1.2.

8.1.1 Model Based Diagnosis System

The model based diagnosis system is able to detect faults in all sensors. The residuals presented in Section 6.3.4 has shown to be sensitive to most of the faults as they where intended to be. The simulated and injected faults are with few exceptions easy to distinguish from the fault free case in the residuals. Thus, the designed tests shows potential of being useful in a real application. The isolability in the system could however be improved. To be able to use backup filters in a proper manner, it is essential to be able to isolate faults in all sensors that are used in the attitude estimation, i.e., magnetometer, accelerometer, and gyroscope. Thus, a test that is sensitive to faults in the accelerometer and gyroscopes only, would improve the use of the diagnosis system significantly.

A large part of the work have been focused on residual generation and evaluation of tests in MATLAB. From the evaluation of the individual tests it can be concluded that the occurrence of a fault is clearly visible in the residuals. It was not possible to test the diagnosis system on the aircraft during a real flight. Hence the tests which included the pressure sensors and the GPS couldn't be evaluated in real-time. Test sensitive of faults in the magnetometer, accelerometer, and gy-

roscope has though been evaluated on the EasyPilot, in an indoor environment. These tests showed good results when using a CUSUM algorithm for fault detection. It is however hard to confirm that these test works properly during a real flight since vibrations and magnetic disturbances on the aircraft could give rise to false alarms.

As mentioned in Section 1.3, it is desirable to minimize any added effort of tuning the diagnosis system on the EasyPilot. Together with the CUSUM test, the designed system only contains two tuning parameters per test. Furthermore, the designed tests, apart from test $\delta_{3,1}$ which contains an EKF, are straightforward to implement both in MATLAB and C. An evaluation of the computational complexity of the designed diagnostic tests have been outside the scope of this thesis. However, the computations related to the diagnosis system have not forced the main loop on the autopilot to fall below 120 Hz, which is the frequency used in the system.

The advantages with the MBDS compared to the TRA are in particular the light weight and the lower cost. The MBDS could advantageously be useful in small UAVs where the weight of the system often is critical.

8.1.2 Triple Redundant Autopilot

All work with the triple redundant autopilot system has been done using three EasyPilots and a supervisor component. In a diagnosis point of view the task of designing residual generators in the TRA has not been as time consuming as in the MBDS, since the hardware redundancy provides full isolability and corresponds to trivial residual generators. Hence a large part of the work with the triple redundant autopilot has been focused on hardware communication as CAN and USART. Since no logged data has been available for evaluation, the system has been developed as a real-time system in C. Since communication with the ground control station through the modem is not implemented it is not possible to evaluate the system during a real flight.

The CUSUM algorithm has shown to work good as fault detection algorithm together with the residual generators. The evaluation of the residuals have been poor due to lack of data logging functionality in the system. The practical experiments that have been performed as evaluation of the tests indicates that the tests are sensitive to the faults as supposed. The properties of the residuals have however not been evaluated any further. It would have been interesting to model the triple redundant autopilot in Simulink or Modelica, and evaluate the performance in a simulator.

Due to the hardware redundancy, a fully developed TRA have higher reliability than the MBDS. Typical applications where the TRA could be useful are:

- Expensive airframes or payloads
- High risk missions
- Missions in populated areas

8.2 Future Work

This section presents ideas for future work which have arisen during the work with this thesis. Both practical improvements for further development of the system and things that would be interesting to analyze from a more theoretical point of view are presented in this section.

8.2.1 Improved Isolability

In a diagnosis point of view it would be desirable to obtain full isolability in the MBDS. In particular, the final set of tests should be augmented with a test sensitive to faults in the accelerometers and gyroscopes but not to faults in the magnetometer. A framework for residual generation by computing unknown variables in a set of equations, according to a computation sequence is presented in Svard and Nyberg [2010]. It would be interesting to investigate if residuals with desirable fault sensitivity could be generated using this framework.

From a theoretical perspective it would have been interesting to compare a complete set of tests designed according to the framework in Svard and Nyberg [2010] or any similar method, with the proposed set of tests in this thesis.

8.2.2 Other Fault Sources

The reliability of the UAV can be further improved by taking other fault sources than sensor faults into account. Faults in electrical components, the power supply and the actuator can be as devastating as faults in the sensors. Hence it would be desirable to take those fault sources into account in the diagnosis system as well.

8.2.3 Multiple Faults

Only single faults have been taken into account in this thesis. It would be interesting to take multiple faults into account as well, to analyze how the detectability of a new fault is affected if the system already is in a fault mode.

8.2.4 Backup Filter

The diagnosis system developed in this thesis does not take fault handling into account. It would be desirable to have a set of backup filters that could be used in situations where faults are present in any of the sensors that updates the current attitude estimation filter. Using a backup filter, the UAV might be able to continue its mission or at least be able to return to the home waypoint in a safe manner. The EKF presented in Section 6.3.4 could for example be used as a backup filter for attitude estimation.

8.2.5 Simulator and Simulink Model

To facilitate further development and improvements of the Triple Redundant Autopilot it would be useful to have a Simulink model of the autopilot. Together with a simulator the Simulink model would be a helpful tool in the development process.

A

Appendix

A.1 Vincenty's Formula

The central angle between two points on a sphere is given by Vincenty's formula (Equation A.1), presented in Vincenty [1975].

$$\Delta\hat{\sigma} = \arctan \left(\frac{\sqrt{(\cos\phi_f \sin\Delta\lambda)^2 + (\cos\phi_s \sin\phi_f - \sin\phi_s \cos\phi_f \cos\Delta\lambda)^2}}{\sin\phi_s \sin\phi_f + \cos\phi_s \cos\phi_f \cos\Delta\lambda} \right) \quad (\text{A.1})$$

Where ϕ_f, λ_f and ϕ_s, λ_s is the geodetic latitude and longitude for two points on a sphere and $\Delta\phi, \Delta\lambda$ is their absolute differences.

A.2 Plots

In this section plots of residuals, test quantities, and measured signals from the model based diagnosis system in Section 6 will be presented. Descriptions of the specific plots is found in the captions.

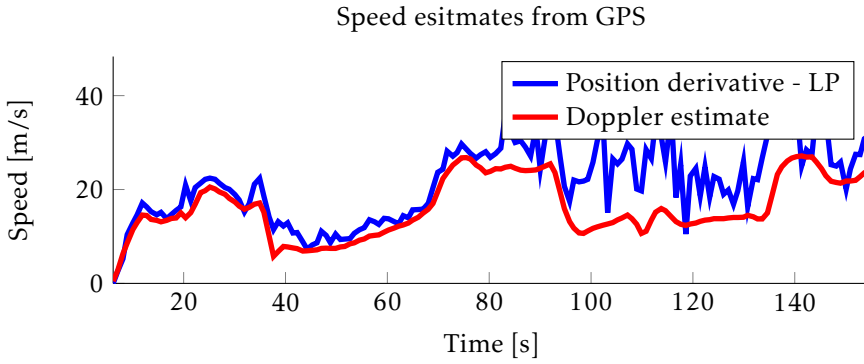


Figure A.1: The speed indicated by the GPS and the estimated speed from the position estimates given by the GPS. The indicated speed from the GPS is based on tracking the frequency of the received messages, using the doppler effect. At time $t = 80$ a variance fault in the position estimate is injected.

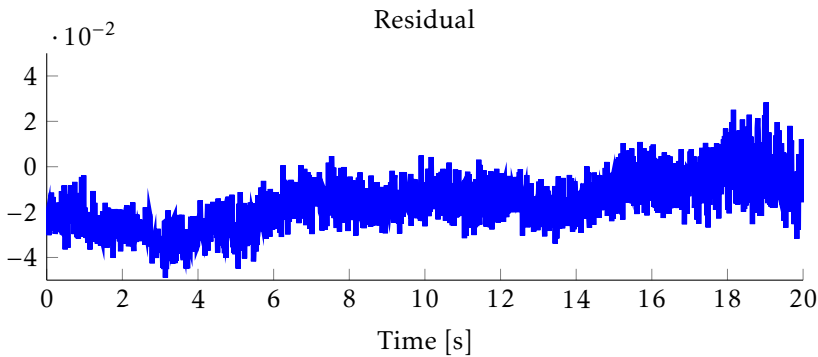


Figure A.2: The residual of test $\delta_{2,1}$ in the fault free case from a logged dataset. The residual is alternating around zero when no fault is present.

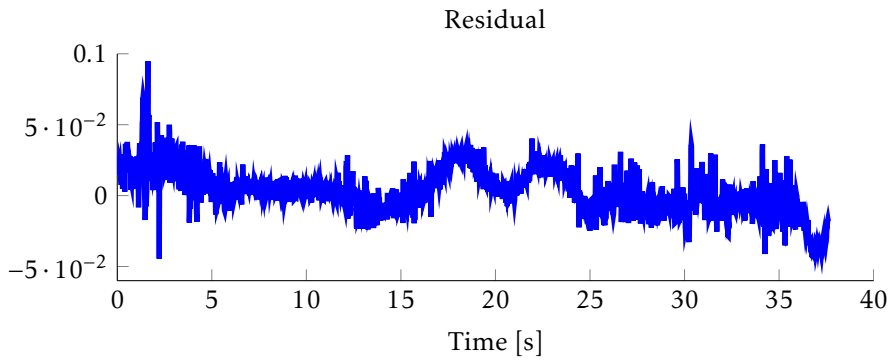


Figure A.3: The residual of test $\delta_{3,1}$ in the fault free case from a logged dataset. The residual is alternating around zero when no fault is present.

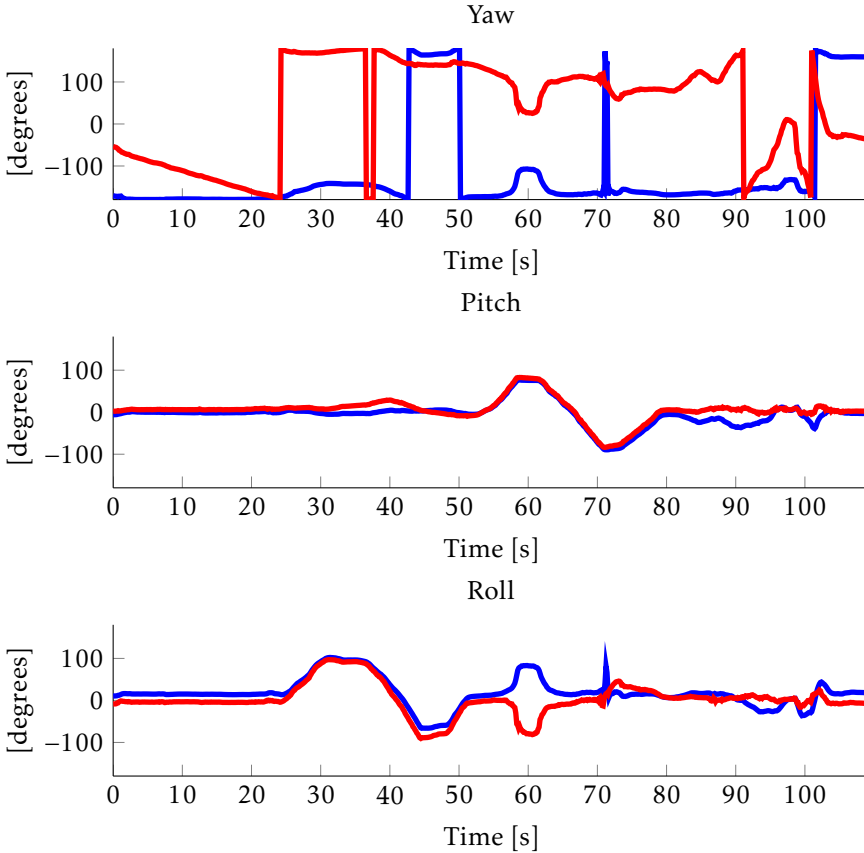


Figure A.4: Estimated orientation by the filter and the proposed backup filter used in test $\delta_{3,1}$. The blue line is the estimate by the magnetic EKF and the red line is the estimate from the filter on the autopilot. The Yaw estimation error is large compared to the pitch and the roll errors since the magnetic field vector of the Earth is almost parallel to the z-axis, and hence the Yaw-angle is hard to estimate by the EKF. As seen in Figure A.4, the aircraft is pitched up to 90 degrees at time $t \in [57, 63]$. With 90 degrees pitch the magnetic field vector is almost parallel with the x-axis, hence the estimate of the roll angle will be poor, which can be seen in Figure 6.4. In real applications the aircraft spend most time in level mode, in which the pitch angle and roll angle are small. During level mode, the estimated pitch and roll could be used as a backup filter together with the heading estimate from the GPS which is more accurate than the yaw estimate from the EKF.

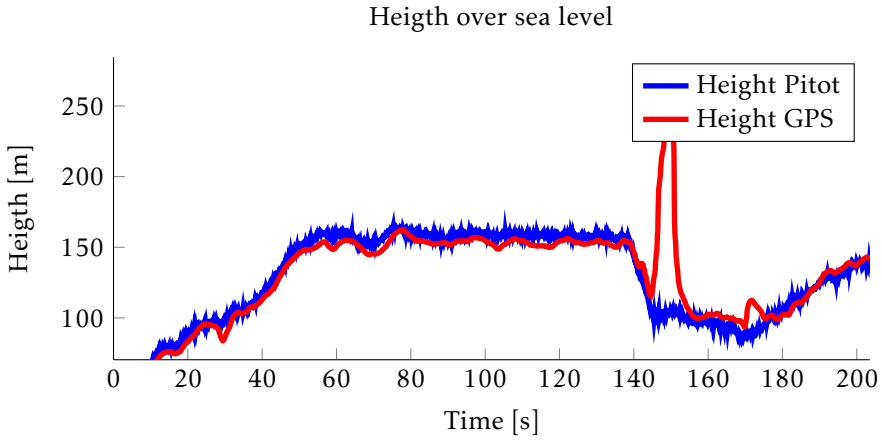


Figure A.5: Estimated heigth over sea level by the GPS and the static pressure sensor during a flight. The estimate from the GPS varies more than the estimate from the static pressure sensor, but the estimate from the GPS does not have an offset. To get a good estimate of the true altitude the RLS approach for estimating K presented in Magnusson [2013] can be used. The RLS approach is however dependent on a reliable estimate from the GPS. As seen in Figure A.5 the GPS indicates an abrupt increase of the altitude after approximately 150 seconds

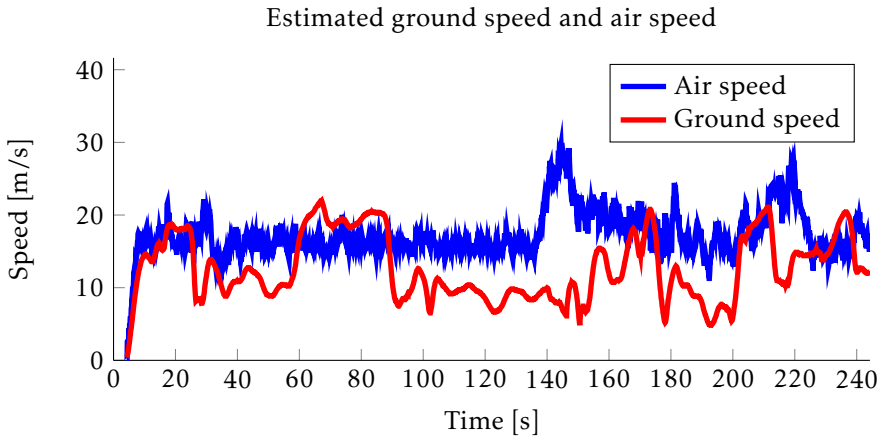


Figure A.6: Estimated air speed and ground speed during a flight.

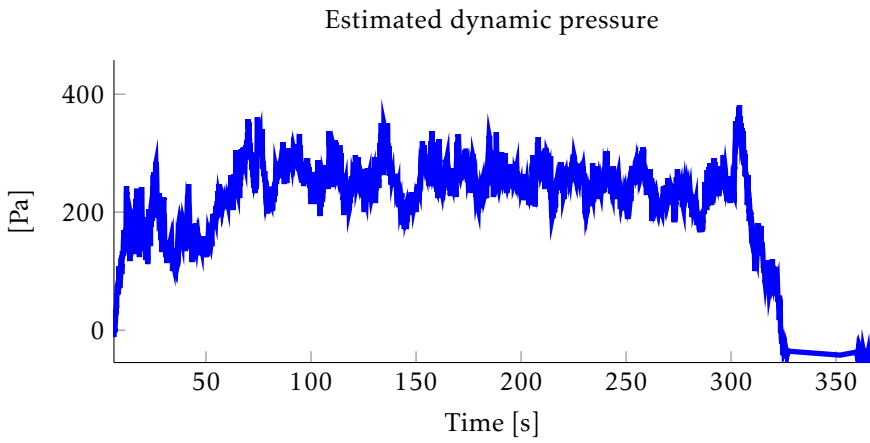


Figure A.7: Estimated dynamic pressure during a flight.

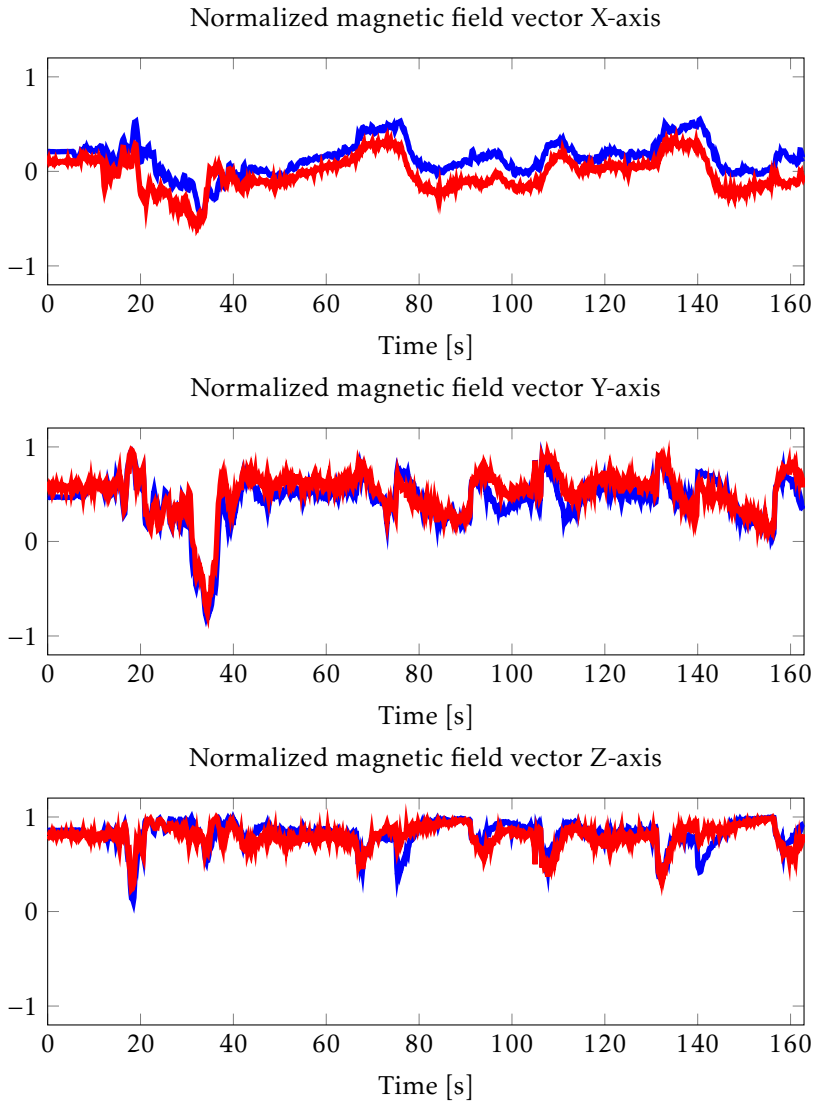


Figure A.8: Normalized magnetometer measurements and rotated magnetic reference vector in the NED-frame. The red line represents calibrated measurements from the magnetometer and the blue line is the rotated magnetic reference vector.

Bibliography

- M. Blanke. *Diagnosis and Fault-Tolerant Control*. Engineering online library. Springer London, Limited, 2003. ISBN 9783540010562. URL <http://books.google.se/books?id=j4Hm3f2NAvIC>. Cited on page 7.
- Tom Chalko. High accuracy speed measurement using gps (global positioning system). *Nujournal*, 2007. Cited on page 39.
- Haiyang Chao, Yongcan Cao, and YangQuan Chen. Autopilots for small fixed-wing unmanned air vehicles: A survey. In *Mechatronics and Automation, 2007. ICMA 2007. International Conference on*, pages 3144–3149, aug. 2007. doi: 10.1109/ICMA.2007.4304064. Cited on page 6.
- M. Euston, P. Coote, R. Mahony, Jonghyuk Kim, and T. Hamel. A complementary filter for attitude estimation of a fixed-wing uav. In *Intelligent Robots and Systems, 2008. IROS 2008. IEEE/RSJ International Conference on*, pages 340–345, sept. 2008. doi: 10.1109/IROS.2008.4650766. Cited on page 42.
- S. Gururajan, A. McGrail, Y. Gu, B. Seanor, M.R. Napolitano, J. Prucz, and K. Philips. Identification of aerodynamic parameters for a small uav from flight data. volume 2, pages 1005–1019, 2012. URL <http://www.scopus.com/inward/record.url?eid=2-s2.0-84866983957&partnerID=40&md5=efe555ae9723de4268310b1891261adf>. Cited on page 6.
- F. Gustafsson. *Adaptive filtering and change detection*. Wiley, 2000. ISBN 9780471492870. URL <http://books.google.se/books?id=cyNTAAAMAAJ>. Cited on page 20.
- F. Gustafsson. *Statistical Sensor Fusion*. Utbildningshuset/Studentlitteratur, 2010. ISBN 9789144054896. URL http://books.google.se/books?id=yd_2SAAACAAJ. Cited on pages 7, 33, and 39.
- William R. Hamilton. On a new species of imaginary quantities connected with a theory of quaternions. *Proceedings of the Royal Irish Academy*, 1843. Cited on page 26.
- G. Heredia, A. Ollero, R. Mahtani, M. Béjar, V. Remuß, and M. Musial.

- Detection of sensor faults in autonomous helicopters. volume 2005, pages 2229–2234, 2005. URL <http://www.scopus.com/inward/record.url?eid=2-s2.0-33846177577&partnerID=40&md5=ccd4cdd428bd44ffbddbf4e98636c4e8>. cited By (since 1996) 9. Cited on page 7.
- National Imagery and Mapping Agency. Technical report 8350.2 third edition, 2000. Cited on page 23.
- Gang Xu STMicroelectronics Jay Esfandyari, Roberto De Nuccio. Introduction to mems gyroscopes. *Solid State Technology*, 2010. URL <http://www.electroiq.com/articles/stm/2010/11/introduction-to-mems-gyroscopes.html>. Cited on page 31.
- Yeonsik Kang and J.K. Hedrick. Linear tracking for a fixed-wing uav using nonlinear model predictive control. *Control Systems Technology, IEEE Transactions on*, 17(5):1202–1210, sept. 2009. ISSN 1063-6536. doi: 10.1109/TCST.2008.2004878. Cited on page 6.
- M. Kayton and W.R. Fried. *Avionics Navigation Systems*. A Wiley-Interscience publication. John Wiley & Sons, 1997. ISBN 9780471547952. URL <http://books.google.se/books?id=1KLTUWLz8jcC>. Cited on page 23.
- Mattias Krysander, J. Åslund, and Mattias Nyberg. An efficient algorithm for finding minimal overconstrained subsystems for model-based diagnosis. *Systems, Man and Cybernetics, Part A: Systems and Humans, IEEE Transactions on*, 38(1):197–206, 2008. ISSN 1083-4427. doi: 10.1109/TSMCA.2007.909555. Cited on page 18.
- Mattias Krysander, Jan Åslund, and Erik Frisk. A structural algorithm for finding testable sub-models and multiple fault isolability analysis. 21st International Workshop on Principles of Diagnosis (DX-10), Portland, Oregon, USA, 2010. Cited on pages 17, 18, and 19.
- G. Latif-Shabgahi, J.M. Bass, and S. Bennett. A taxonomy for software voting algorithms used in safety-critical systems. *IEEE Transactions on Reliability*, 53(3):319–328, 2004. URL <http://www.scopus.com/inward/record.url?eid=2-s2.0-2442465295&partnerID=40&md5=6eada7b58038648bbf6d1202775d741e>. cited By (since 1996) 46. Cited on page 74.
- R.R. Lima and L.A.B. Tôrres. Performance evaluation of attitude estimation algorithms in the design of an ahrs for fixed wing uavs. pages 255–260, 2012. URL <http://www.scopus.com/inward/record.url?eid=2-s2.0-84871588346&partnerID=40&md5=84a4a51b1f2d5d6d06932b3d0785e98b>. cited By (since 1996) 0. Cited on page 6.
- H.J. Luinge, P.H. Veltink, and C.T.M. Baten. Estimation of orientation with gyroscopes and accelerometers. In *[Engineering in Medicine and Biology, 1999]*.

- 21st Annual Conference and the 1999 Annual Fall Meeting of the Biomedical Engineering Society] BMES/EMBS Conference, 1999. Proceedings of the First Joint*, volume 2, page 844 vol.2, oct 1999. doi: 10.1109/IEMBS.1999.803999. Cited on page 46.
- Thom Magnusson. State estimation of uav using extended kalman filter. Master's thesis, Linköping University, 2013. Cited on pages 6, 23, 31, 32, 33, 35, 37, 41, 44, 45, 58, 61, and 85.
- S.M. Magrabi and P.W. Gibbens. Decentralised fault detection and diagnosis in navigation systems for unmanned aerial vehicles. In *Position Location and Navigation Symposium, IEEE 2000*, pages 363 –370, 2000. doi: 10.1109/PLANS.2000.838326. Cited on pages 7 and 13.
- Mattias Nyberg. *Model Based Fault Diagnosis: Methods, Theory, and Automotive Engine Applications*. PhD thesis, Linköpings Universitet, June 1999. Cited on pages 13 and 15.
- R. RemenYTE-PreSCott, J.D. Andrews, and P.W.H. Chung. An efficient phased mission reliability analysis for autonomous vehicles. *Reliability Engineering and System Safety*, 95(3):226 – 235, 2010. ISSN 0951-8320. doi: 10.1016/j.res.2009.10.002. URL <http://www.sciencedirect.com/science/article/pii/S0951832009002397>. Cited on page 7.
- Valérie Renaudin, Muhammad Haris Afzal, and Gérard Lachapelle. Complete triaxis magnetometer calibration in the magnetic domain. *Journal of sensors*, 2010, 10 2010. ID 967245. Cited on page 60.
- J.Z. Sasiadek and P. Hartana. Sensor fusion for navigation of an autonomous unmanned aerial vehicle. volume 2004, pages 4029–4034, 2004. URL <http://www.scopus.com/inward/record.url?eid=2-s2.0-3042586228&partnerID=40&md5=a64d24f9d64894365170c921db9083ae>. cited By (since 1996) 10. Cited on page 7.
- Malcolm D. Shuster. Survey of attitude representations. *Journal of the Astronautical Sciences*, 41(4):439–517, 1993. ISSN 00219142. URL <http://www.scopus.com/inward/record.url?eid=2-s2.0-0027685324&partnerID=40&md5=564003a9a7e7fb56de7d74c45c1da8b9>. cited By (since 1996) 634. Cited on pages 25 and 28.
- Sensors Spectrum and Controls Inc. Compensating for accelerometer misalignments. tech note 413. 2010. Cited on page 33.
- Carl Svard and Mattias Nyberg. Residual generators for fault diagnosis using computation sequences with mixed causality applied to automotive systems. *Systems, Man and Cybernetics, Part A: Systems and Humans, IEEE Transactions on*, 40(6):1310–1328, 2010. ISSN 1083-4427. doi: 10.1109/TSMCA.2010.2049993. Cited on pages 18 and 79.

- Alejandro Dzul Tadeo Espinoza and Miguel Llama. Linear and non-linear controllers applied to fixed-wing uav. In *International Journal of Advanced Robotic Systems*, Andon Topalov (Ed.), 2013. doi: 10.5772/53616. URL http://www.intechopen.com/journals/international_journal_of_advanced_robotic_systems/linear-and-nonlinear-controllers-applied-to-fixed-wing-ua. Cited on page 6.
- Texas-Instruments. Introduction to controller area network (can), 2008. Cited on page 71.
- D.H. Titterton, J.L. Weston, and Institution of Electrical Engineers. *Strapdown Inertial Navigation Technology, 2nd Edition*. Iee Radar Series. The Institution of Engineering and Technology, 2004. ISBN 9780863413582. URL <http://books.google.se/books?id=WwrCrn54n5cC>. Cited on page 33.
- Törnqvist. *Statistical Fault Detection with Applications to IMU Disturbances*. PhD thesis, Linköping University, 2006. Cited on page 26.
- Clas Veiback. Automatic control of unmanned aerial vehicles. Master's thesis, Uppsala University, 2010. Cited on pages 6, 23, 31, 41, 45, 58, and 64.
- Venkat Venkatasubramanian, Raghunathan Rengaswamy, Kewen Yin, and Surya N. Kavuri. A review of process fault detection and diagnosis: Part i: Quantitative model-based methods. *Computers And Chemical Engineering*, 27(3):293 – 311, 2003. ISSN 0098-1354. doi: 10.1016/S0098-1354(02)00160-6. URL <http://www.sciencedirect.com/science/article/pii/S0098135402001606>. Cited on page 13.
- Thaddeus Vincenty. Direct and inverse solutions of geodesics on the ellipsoid with application of nested equations. *Survey review*, 23(176):88–93, 1975. Cited on page 81.



Upphovsrätt

Detta dokument hålls tillgängligt på Internet — eller dess framtida ersättare — under 25 år från publiceringsdatum under förutsättning att inga extraordinära omständigheter uppstår.

Tillgång till dokumentet innebär tillstånd för var och en att läsa, ladda ner, skriva ut enstaka kopior för enskilt bruk och att använda det oförändrat för icke-kommersiell forskning och för undervisning. Överföring av upphovsrätten vid en senare tidpunkt kan inte upphäva detta tillstånd. All annan användning av dokumentet kräver upphovsmannens medgivande. För att garantera äktheten, säkerheten och tillgängligheten finns det lösningar av teknisk och administrativ art.

Upphovsmannens ideella rätt innefattar rätt att bli nämnd som upphovsman i den omfattning som god sed kräver vid användning av dokumentet på ovan beskrivna sätt samt skydd mot att dokumentet ändras eller presenteras i sådan form eller i sådant sammanhang som är kränkande för upphovsmannens litterära eller konstnärliga anseende eller egenart.

För ytterligare information om Linköping University Electronic Press se förlagets hemsida <http://www.ep.liu.se/>

Copyright

The publishers will keep this document online on the Internet — or its possible replacement — for a period of 25 years from the date of publication barring exceptional circumstances.

The online availability of the document implies a permanent permission for anyone to read, to download, to print out single copies for his/her own use and to use it unchanged for any non-commercial research and educational purpose. Subsequent transfers of copyright cannot revoke this permission. All other uses of the document are conditional on the consent of the copyright owner. The publisher has taken technical and administrative measures to assure authenticity, security and accessibility.

According to intellectual property law the author has the right to be mentioned when his/her work is accessed as described above and to be protected against infringement.

For additional information about the Linköping University Electronic Press and its procedures for publication and for assurance of document integrity, please refer to its www home page: <http://www.ep.liu.se/>